

Probing Polaritons in 2D Materials

Cheng Luo, Xiangdong Guo, Hai Hu, Debo Hu, Chenchen Wu, Xiaoxia Yang,*
and Qing Dai*

Polaritons in 2D materials exhibit extensive optical phenomena, such as an ultrahigh field confinement and tunability and, thus, have been attracting increasing attentions. Many different methods have been developed to characterize and manipulate polaritons, which in turn has promoted a steady booming of this field. Here, the significant progress made in probing polaritons in 2D materials based on the characterization method, i.e., optical far-field, optical near-field, and (opto)electronic methods is reviewed. Perspectives on the potential development and applications of these methods are also discussed.

1. Introduction

Polaritons are electromagnetic quasiparticles derived from coupling photons with elementary electric dipoles.^[1] For example, plasmon polaritons arise from the collective movement of free carriers, exciton polaritons from the movement of electron hole pairs in a wave fashion, and phonon polaritons from the atomic vibrations of polar insulators.^[2] Polaritons can break the diffraction limit and manipulate light on a nanoscale, making them promising for nanophotonics. For 2D materials, a full set of polaritons sharing the principal advantage of an ultrahigh confinement on electromagnetic energy can be supported. These polaritons in 2D materials (2D polaritons) offer a promising platform for strong light–matter interactions and nanoscale light manipulation. Numerous functions of 2D polaritons have been demonstrated, including surface-enhanced infrared absorption, ultrafast plasmonic modulation, ultra-small phase modulation, ultraslow light propagation, metasurface engineering, and hyper-focusing lenses. These properties and devices are highly useful in nanophotonics and optoelectronics.^[3–7]

C. Luo, X. Guo, Dr. H. Hu, Dr. D. Hu, C. Wu, Prof. X. Yang, Prof. Q. Dai
Division of Nanophotonics
CAS Key Laboratory of Standardization and Measurement
for Nanotechnology
CAS Center for Excellence in Nanoscience
National Center for Nanoscience and Technology
Beijing 100190, China
E-mail: yangxx@nanocr.cn; daiq@nanocr.cn

C. Luo, X. Guo, Dr. H. Hu, Dr. D. Hu, C. Wu, Prof. X. Yang, Prof. Q. Dai
Center of Materials Science and Optoelectronics Engineering
University of Chinese Academy of Sciences
Beijing 100049, China

 The ORCID identification number(s) for the author(s) of this article can be found under <https://doi.org/10.1002/adom.201901416>.

DOI: 10.1002/adom.201901416

Over the past decade, 2D polaritons, especially graphene plasmons and hexagonal boron nitride (h-BN) phonon polaritons, have been widely explored both theoretically and experimentally. This fast development was facilitated by both the fabrication of 2D materials and progress in probing methods. For example, scattering scanning near-field optical microscopy (s-SNOM) allows imaging of propagating polaritons in real space with ultra-high spatial resolution (<30 nm), which is defined by the s-SNOM tip radii and not related to the light wavelength.^[8–10] The in

situ background subtraction enables highly sensitive infrared spectroscopy so that the weak absorption of polaritons in monolayer graphene and h-BN layers can be detected.^[11] The development of high-resolution electron energy loss spectroscopy (EELS) has enabled the detection of h-BN phonon polaritons around 100 meV.^[12]

Different probing methods each have strengths and weaknesses that are complementary to one another for the detection of 2D polaritons. For example, far-field infrared spectroscopy can cover a broad spectral range and is easily performed, but its spatial resolution is limited by the Abbe diffraction and the sensitivity of the infrared spectroscopy is weak. The s-SNOM method has ultra-high spatial resolution, but the excitation efficiency is low due to the large wavevector mismatch of the highly confined 2D polaritons.^[11] Electronic methods have even higher spatial resolution than optical methods due to the short de Broglie wavelength, but the low-energy polaritons are hard to distinguish because of the energy extension of the incident electron beam.^[13] A comparison and cautious selection of these techniques should be performed prior to characterizing different 2D polaritons. Importantly, the properties of 2D materials and their polaritons vary across materials, making the selection of probing method critical. Different electromagnetic spectrum responses also require the coverage of different probing methods to be considered for different polaritons.^[1]

In this article, we review the available techniques for 2D polariton characterization in terms of the optical far-field, optical near-field, and (opto)electronic methods. First, we discuss the optical far-field methods, which are exhausted by overcoming wavevector mismatch, using techniques such as diffraction gratings, attenuated total reflection (ATR), and all-optical nonlinear wave mixing. Next, near-field optical methods, including s-SNOM, photothermal-induced resonance microscopy (PTIR), peak force infrared microscopy (PFIR), and photo-induced force microscopy (PiFM), are discussed. Subsequently, the electronic methods are discussed, where EELS is the main

focus, cathodoluminescence (CL), photoemission electron microscopy (PEEM), and photo-induced near-field electron microscopy (PINEM) are also discussed. Finally, we review the current challenges and present perspectives for probing 2D polaritons. By describing the underlying physical mechanisms and highlighting the individual strengths and limitations of each method, we intend to convey an intuitive understanding of their applicability for 2D polaritons. **Figure 1** presents a summary of examples^[8,12,14–40] of these techniques for probing polaritons in 2D materials.

2. Far-Field Optical Methods

The oldest technique of probing polaritons, the far-field optical method, covers a broad spectrum and is easy to perform, making it widely used for probing polaritons. The key challenge when measuring 2D polaritons using the far-field method is overcoming wavevector mismatch between free space electromagnetic waves and highly confined polaritons. To solve this problem, the following several methods have been developed.

2.1. Diffraction Gratings and Subdiffractive Nanostructures

Diffraction on a periodic structure can be coupled to transverse magnetic (TM) light via the grating scattering vector, which provides extra momentum to excite polaritons.^[41,42] This momentum matching can be defined by the size and period of the grating and incident angle. Enabling materials with periodic grating structures is the most commonly used method for far-field excitation of polaritons.^[43–45] With the development of modern nanostructure processing, polaritons can be manipulated from the visible to THz spectral regions.

A ribbon array, also known as a diffraction grating, is the simplest sub-wavelength structure for exciting infrared or THz



Cheng Luo is a Ph.D. student working under Prof. Qing Dai's supervision in the National Center of Nanoscience and Technology, China. His main research focuses on 2D materials and nanophotonics.



Qing Dai is a professor of the National Center of Nanoscience and Technology, China. He received his B.Eng. and M.Eng. in electronic and electrical engineering from Imperial College, London in 2007 and Ph.D. in nano photonics from the Department of Engineering, University of Cambridge in 2011. His main research interests are low-dimensional materials, optoelectronics, nanophotonics, and near-field optical characterization.

polaritons. **Figure 2a** shows a diffraction grating configuration. When a beam of light illuminates the structure, light waves with various wavevectors are produced and polaritons become excited when both the frequency and wavevector of the light match or coincide with the polaritons in the materials.^[46] In

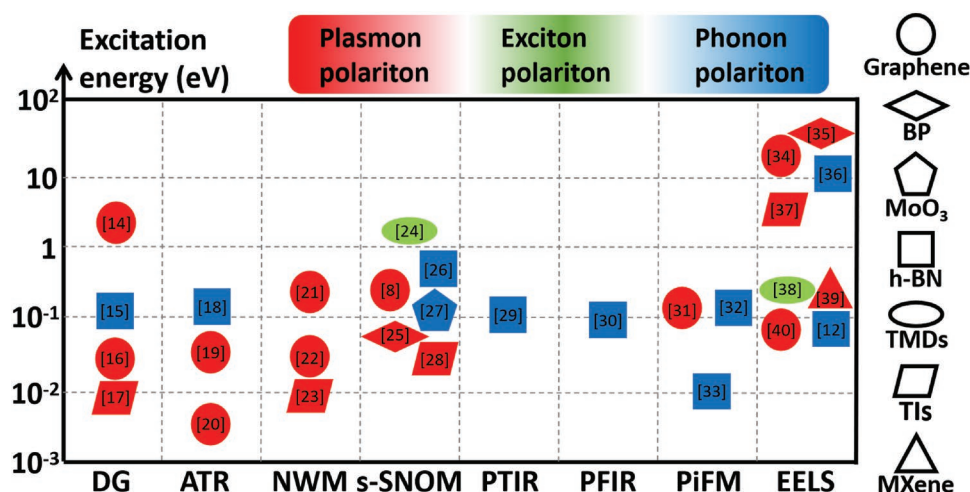


Figure 1. Representative examples of 2D material polaritons probed by various techniques, including diffraction gratings (DG), attenuated total reflection (ATR), nonlinear wave mixing (NWM), scattering scanning near-field optical microscopy (s-SNOM), photothermal-induced resonance microscopy (PTIR), peak force infrared microscopy (PFIR), photo-induced force microscopy (PiFM), electron energy loss spectroscopy (EELS). BP, black phosphorus; TMDs, transition metal dichalcogenides; TIs, topological insulators. The red, green, and blue colors indicate plasmon, exciton, and phonon polaritons, respectively. The values are extracted from references as marked in the patterns.

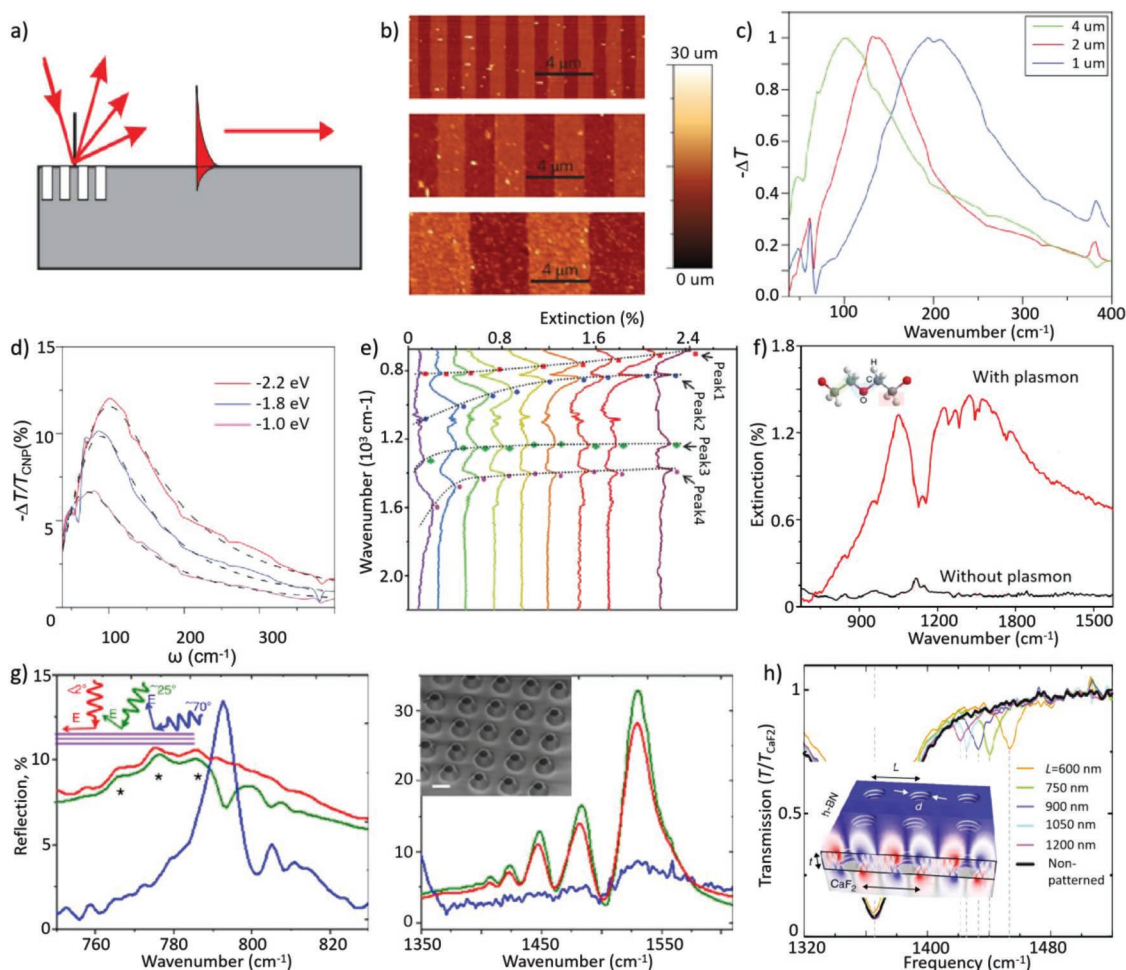


Figure 2. Diffraction grating structures for exciting polaritons and their applications. a) Schematic diagram of diffraction grating for wavevector compensation. Reproduced with permission.^[46] Copyright 2004, Elsevier B.V. b) AFM images of graphene micro-ribbon arrays with various periods. c) Transmission spectra for different graphene micro-ribbon widths at the same doping concentration. d) Control of THz resonance of plasmon excitations through electrical gating. b–d) Reproduced with permission.^[16] Copyright 2011, Springer Nature. e) The extinction spectra of the graphene/h-BN device with different graphene ribbon widths. Reproduced with permission.^[53] Copyright 2016, Wiley-VCH. f) Highly sensitive detection of molecular vibration fingerprints with graphene plasmon. Reproduced with permission.^[54] Copyright 2016, Springer Nature. g) Fourier transform infrared spectroscopy (FTIR) reflection spectra of the lower (left) and upper (right) Reststrahlen bands collected from a periodic subdiffraction nanostructure array at three incident angles. Inset: a schematic of these measurements (left) and a SEM image of a h-BN nanoresonator array (right). Reproduced with permission.^[60] Copyright 2014, Springer Nature. h) Normalized transmission spectra for the phonon polaritonic crystal based on h-BN hole arrays with period L ranging from 600 to 1200 nm. Inset: schematic of a hole array in a h-BN slab on a CaF_2 substrate. Reproduced with permission.^[50] Copyright 2019, Springer Nature.

2011, Ju et al.^[16] demonstrated etched graphene micro-ribbon arrays (as shown in Figure 2b) allow electromagnetic radiation to excite plasmons with wavevector $q \approx (2n + 1)\pi/w$ (where w is the width of the ribbon and $n = 0, 1, 2, \dots$). The collective oscillations of electrons across the width of the ribbons are induced by the incident electric field, which results in absorption of the transmission spectra. Graphene plasmon resonances in micro-ribbon arrays can be tuned over a broad THz frequency range by changing the ribbon widths (Figure 2c). In addition, the supported plasmons can be also controlled via in situ electrostatic doping due to the tunability of the graphene Fermi level (Figure 2d).

Due to the development of nanostructures processing, gratings can be smaller in size and polaritons can be tuned to higher spectral regions. In 2013, Yan et al.^[47] etched graphene into nanoribbons with dimensions as small as 50 nm

and observed mid-infrared (4–15 μm) plasmon polaritons. Brar et al.^[43] observed plasmon resonances up to 2500 cm^{-1} by tuning the ribbon width (down to 15 nm) and graphene charge density. Diffraction gratings structures have also proved suitable for polaritons excitation in other 2D materials. For example, Liu et al.^[48] showed localized surface plasmon resonances at mid-infrared and far-infrared wavelengths in black phosphorus (BP) nanoribbon and nanopatch arrays. Phonon polaritons have also been measured in h-BN nanoribbons.^[15]

In addition to molding materials into grating structures, introducing diffraction gratings beneath or above materials can also excite polaritons. For example, Gao et al.^[49] showed graphene plasmons in the infrared wavelength region can be excited by silicon diffractive grating.

The tunability of diffraction gratings based on structure design helps facilitate the use of polaritons in a lot of

applications involving the detection of chemical signals,^[50] as well as identifying the hybridization of different polaritons. By pushing graphene plasmon polaritons to the mid-infrared, Brar et al.,^[51] Jia et al.,^[52] and Yang et al.^[53] discovered hybridization of graphene plasmons and phonon polaritons in h-BN sheets. As shown in Figure 2e, Yang et al. used plasmon in graphene ribbons to couple with phonon polaritons in h-BN. Hu et al.^[54] demonstrated in situ electrically tunable graphene plasmon allows molecular fingerprinting at the nanoscale level with nanoribbon structures (Figure 2f).

Subdiffractive nanostructures, which feature ultrahigh confinement of light at lengths much shorter than the diffraction limits, are the other important structures designed for far-field optical detections. Distinct from diffraction gratings that can produce propagating polaritons, subdiffractive nanostructures support only localized polaritons. Many attempts of subdiffraction confinement of light are based on metallic nanostructures such as graphene nanodisks^[55,56] and the nanoribbons discussed above that generate localized plasmon polaritons, and polar dielectrics nanostructures, like SiC nanopillars,^[57,58] that support localized phonon polaritons with relatively low loss. In recent years, scientists found the naturally hyperbolic material h-BN displays high light confinement because of its low-loss and hyperbolic properties.^[59] Caldwell et al.^[60] fabricated nanocone array from boron nitride flake and observed four series phonon polariton modes supported in three-dimensionally confined phonon polaritons under optical reflection and transmission measurement, where the resonant modes had extraordinarily high-quality factors up to 283. Figure 2g shows the Fourier transform infrared spectroscopy (FTIR) reflection spectra of the BN nanocones arrays in the lower (left) and upper (right) Reststrahlen bands, respectively. In 2018, Autore et al.^[15] took advantage of the large-quality factors of phonon polaritons in h-BN nanoribbons to realize molecular vibrational spectroscopy. In addition, subdiffractive nanostructures, which display high confinement of light, can also enhance nonlinear optical effects within these structures.^[58,61,62]

Polaritonic crystals are special structure with periodic variations of the refractive index comparable to polariton wavelengths for propagating nano-light. Because of the high confinement of polaritons, polaritonic crystals can manipulate the flow of light at subwavelength scale and enhance light-matter interactions more efficiently than conventional photonic crystals.^[63,64] Various polaritonic crystals have been realized based on several 2D materials. In 2014, Yeung et al.^[65] fabricated period hexagonal lattice holes in graphene and realized selective excitation of plasmons. In 2018, Sunku et al.^[66] overlaid two graphene layers to obtain moiré superlattice. By twisting the two layers of graphene at a small angle, a plasmon photonic crystal was formed. One year later, Alfaro-Mozaz et al.^[50] fabricated phonon polaritonic crystals by engineering a nanoscale hole array in h-BN, which supported ultra-confined phonon polaritons. By changing the period of the array, FTIR characterization revealed the h-BN polaritonic crystal had geometrically tunable Bragg resonances, as shown in Figure 2h.

Diffraction gratings and subdiffractive nanostructures present a simple but practical method for probing 2D polaritons, which promise a broad field of applications in signal detecting

and light manipulating. With this method, the sample quality does not need to be perfect since the average signals are collected from the sample. However, the samples need to be of adequate size, which usually means being at least comparable to the wavelength of the testing light (up to hundreds of micrometers).

2.2. Attenuated Total Reflection

ATR was the first method used to excite plasmon polaritons. Figure 3a presents a schematic diagram of ATR, which corresponds to Kretschman's and Otto's configurations, where the sample is in closely contact with a prism or separated by a dielectric with a thickness of less than one wavelength, respectively. The prism with a larger relative permittivity than the dielectric layer will totally reflect the incident beam once the angle of incidence exceeds the critical angle. The electromagnetic field that is perpendicular to the interface decays exponentially as the wavevector increases, which can therefore be coupled to the surface of the sample and triggers the surface polaritons traveling along the surface. After the above energy transfer process, the intensity of the reflected light decreases radically and the resonance can be observed by measuring the reflectivity, which is tunable by varying the angle of incidence or wavelength.^[67]

In 2010, Bludov et al.^[20] realized a THz switch based on graphene plasmon via an ATR setup. The frequency of the excited plasmon polaritons was as small as a few THz and could be increased by using a prism material with a higher dielectric permeability or gating. Two years later, Gan^[19] showed that by placing highly doped graphene under a high-index coupling prism to increase the refractive index n_p of the prism, a higher frequency (about 10 THz) could be achieved, as shown in Figure 3b. In addition, Menabde et al.^[68] realized probing the surface TE mode in graphene optically by situating graphene between dielectrics with asymmetric indices, and the modified Otto's configuration allows very precise phase matching of the incident wave to the TE excitation. Recently, ATR was also applied to probe the multiple hyperbolic and dielectric modes of h-BN, where phonon polaritons in both the lower and upper Reststrahlen bands were measured with a Kretschmann–Raether configuration. Figure 3c shows a representative *p*-polarized ATR reflectance spectra measured on a 490 nm thick h-BN flake.^[18]

Distinct from diffraction gratings, ATR can overcome the wavevector mismatch with a prism, and, thus, presents a convenient way to probe polaritons without micromachining samples. The polaritons can be tuned using prisms with different dielectric indexes, changing the angle of the incident, and/or controlling the gap between the sample and prism in Otto's configuration.^[69–71] In this respect, ATR is a promising technique for probing polaritons.^[72] However, for monolayer or few-layer 2D materials, especially for their nanostructures, the direct contact with a prism is easy to damage the samples.

2.3. Nonlinear Wave Mixing

Nonlinear optical wave mixing is another method used to excite polaritons. It is a nonlinear optical phenomenon that arises

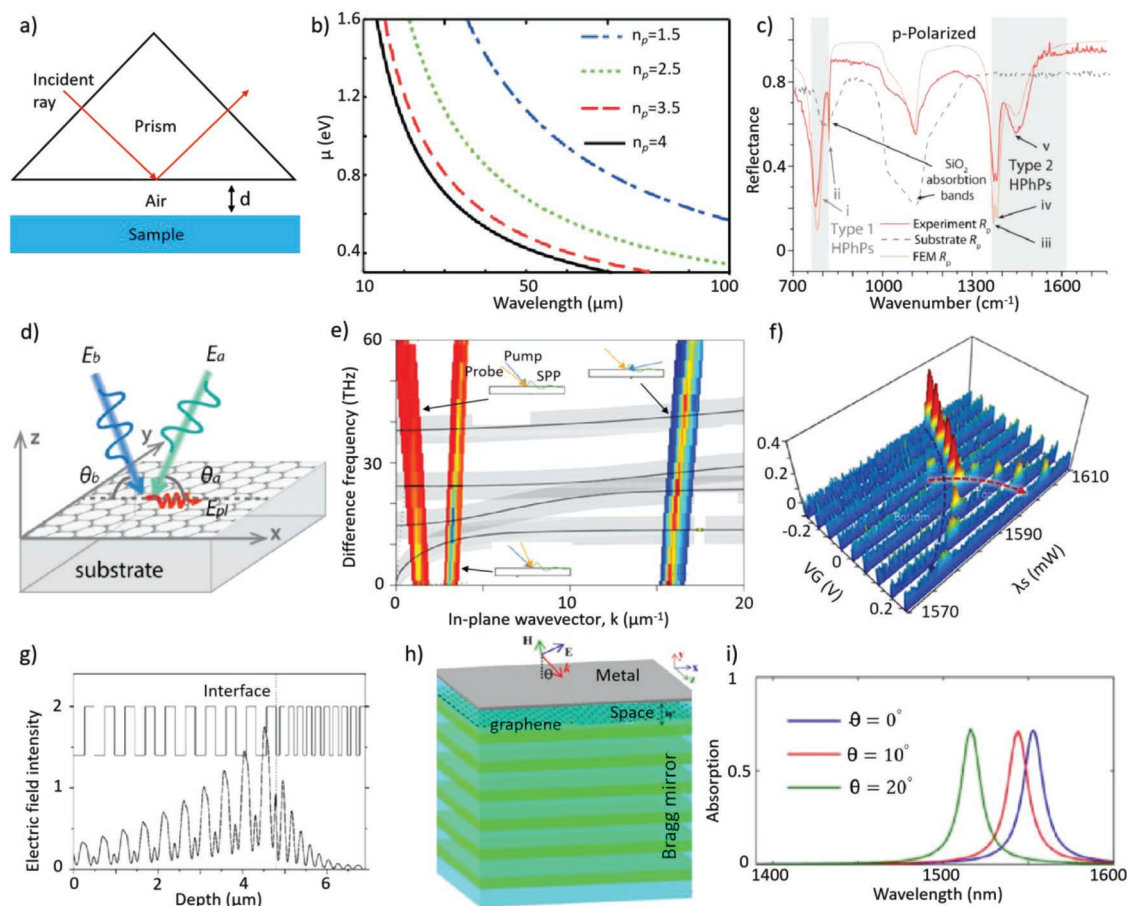


Figure 3. a) Geometry of ATR configuration. The sample in close contact with a prism ($d = 0$) is the Kretschman's configuration, while the sample placed within the evanescent field away from the prism is the Otto's configuration. b) Prism excitation of graphene plasmon-polaritons in the THz range. Reproduced with permission.^[19] Copyright 2012, AIP Publishing. c) p-polarized (red solid curve) ATR micro-spectroscopy measurement of a 490 nm thick h-BN flak. Reproduced with permission.^[18] Copyright 2018, Materials Research Society. d) Geometry of the DFG process. Two pump fields at frequencies ω_a and ω_b incident at angles θ_a and θ_b on sample generate a highly confined polariton wave at their frequency difference and in-plane wave vector $q = q_a - q_b$. Reproduced with permission.^[23] Copyright 2014, American Physical Society (APS). e) Superimposed on the surface plasmon dispersion in three measurement geometries by varying frequency. Reproduced with permission.^[21] Copyright 2015, Springer Nature. f) Gate tunability of the DFG graphene plasmons with V_g increase from -0.2 to 0.2 V. Reproduced with permission.^[22] Copyright 2017, Springer Nature. g) The profile of the electric (solid line) and magnetic (dashed line) fields for a Tamm plasmon at the interface between a metal and periodical dielectric Bragg mirror. Reproduced with permission.^[81] Copyright 2005, APS. h) Sketch of monolayer graphene being inserted into a Tamm plasmon generator. i) Absorption spectra of monolayer graphene at different incident angles θ . The wavelength of the absorption peak exhibits a redshift as the incident angle decreases. h,i) Reproduced with permission.^[86] Copyright 2016, The Optical Society.

from coupling two or more photons, mediated by their interactions with matter, to produce a photon with a frequency that is a linear combination (including second-order effect, third-order effect, etc.) of the original photon frequencies.^[73] Nonlinear optical phenomena exist widely in 2D materials upon interactions with strong optical fields, which have been reviewed in several works.^[74,75] Various works have shown a nonlinear optical effect in graphene with a broad frequency tunability (from near-infrared to THz) and enhancement of the nonlinear optical effect by the material.^[73,76,77]

Difference frequency generation (DFG), a second-order nonlinear optical effect, was recently discovered to trigger plasmon polaritons in graphene and topological insulators (TIs) due to the intrinsic nonlinear optical response of these materials.^[78,79] Figure 3d^[23] presents a schematic diagram of DFG. In this DFG process, two beams with frequencies ω_a and ω_b incident on the sample with well-defined angles θ_a and θ_b provide sufficient in-plane momentum to match the surface plasmon in

graphene. Thus, a highly confined surface plasmon field E_{pl} at their frequency difference and in-plane wavevector $q = q_b - q_a$ can be generated.

Recently, several works confirmed nonlinear wave mixing is a promising technique for probing 2D polaritons. Constant et al.^[21] excited graphene plasmons with a defined wavevector and direction across a large frequency range (up to tens of THz) by controlling the phase matching conditions (Figure 3e). Yao et al.^[22] demonstrated THz graphene plasmons are generated and controllable with a counter-pumped all-optical DFG (Figure 3f). In addition, Yao et al.^[23] showed DFG is also suitable for generating surface plasmons in Bi_2Se_3 (a type of TIs), which has the same massless Dirac fermions feature as graphene.

Nonlinear wave mixing allows for the possibility of all optical excitation of plasmons in 2D materials. For this method, no nanostructures and other equipment need to be prepared and the plasmons can be excited using only irradiating pulses

on the material. An all-optical coupling scheme holds great promise for plasmon sensors or new THz sources.^[80] Up to now, however, the excitation frequency has been limited to the THz range. Although the excitation frequency can be extended to higher or lower frequencies by widening or narrowing the frequency difference of pulses, concurrently eliminating both the wavevector and energy mismatch still poses a major challenge for experiments.

2.4. The Direct Excitation of Tamm Plasmon

Distinct from normal plasmon polaritons, Tamm plasmon is formed between metal and dielectric Bragg mirror, the dispersion of which lies within the light cone and, thus, can be optically excited. Figure 3g shows a common period Bragg mirror configuration,^[81] where the electromagnetic field is strongest at the interface of the metal and dielectric Bragg mirror so that the plasmon can be excited. Importantly, the Tamm state at the interface with the zero in-plane wavevector means both TM and TE polarizations can form Tamm plasmon.^[82] These easily realized modes can be used to enhance light-matter interactions.^[83–85]

The period Bragg mirror configuration can also be used to excite polaritons in 2D materials. In 2016, Lu et al.^[86] excited plasmon polaritons in graphene by inserting monolayer graphene into the silica spacer between a thin metal film and dielectric Bragg mirror (Figure 3h). By placing the graphene properly in the spacer, strong field confinement of Tamm plasmon polaritons in the silica spacer leads to extremely enhanced light absorption (up to 80%) at communication wavelengths. The operating wavelength is also tunable by adjusting the incident angle of light and structure of the Bragg mirror. As shown in Figure 3i, the absorption peak exhibits a redshift as the incident angle decreases. This period structure promises a considerable excitation efficiency because both TM and TE can be used. With this method, there is no need for assistance from external photonic structures, such as optical grating or prisms. Recently, Wang et al.^[87] proposed the edge of terminated graphene serves as an edge-matcher and can compress electromagnetic fields into extremely small mode volume (about 90 times) with remarkable intensity enhancement (about 80 times) by virtue of the graphene plasmonic Tamm state. However, excitation of Tamm plasmon is a rather rarely used method for polaritons excitation because of its lower tunability. Furthermore, the complicated period structure is hard to obtain, which significantly hinders its application. To date, relevant studies for polariton excitation have primarily been computer simulations and calculations.^[88]

2.5. A Summary of Far-Field Optical Methods

Among these far-field optical methods, diffraction gratings powered by modern nanostructure fabrication techniques are the most useful and suitable for characterization of polaritons due to their good accessibility, high tunability, and wide applicability. ATR with prisms raises the wavevector of electromagnetic waves and the frequency of polaritons can be tuned by

adjusting parameters like the light incident angle, refractive index of prism, and sample–prism distance. To date, nonlinear wave mixing has been suitable only for a few types of materials, such as graphene and TIs, and it is hard to be implemented. Tamm plasmon can be directly excited in Bragg mirror configurations, but the complicated structure makes it rarely studied. In addition to the methods discussed above, a great deal of other optical far-field methods, such as light and sound interplay,^[89,90] that can tackle the wavevector mismatch problem are still under exploration.

In general, far-field optical techniques use simple facilities, such as infrared or THz spectrographs. Polaritons are studied indirectly through extinction spectra and the signal tests are quick and simple (usually can be finished in one-step and about one minute). However, a common shortcoming of the far-field optical methods is the spatial resolution is bound by the optical diffraction limit, which is usually in micrometer scale in the infrared frequency range. Moreover, due to the weak light absorption of the atomic thin 2D materials, the sample needs to be large enough to be detectable. Consequently, nanoscale features are spatially indistinguishable in conventional far-field infrared microscopy. In addition, the spectra also suffer from inhomogeneous line broadening due to ensemble averaging within the large sample area.^[30]

3. Optical Near-Field Methods

Detecting optical near-field information makes it possible to bypass the diffraction limit. The near-field signals decay exponentially from the surface and die off within a distance much smaller than the light wavelength. For example, optical information can be collected point-by-point for every image pixel by raster-scanning a probe over the sample surface through scanning near-field optical microscopy (SNOM).^[91] Optical near-field methods have drawn tremendous attention in recent years by promoting the study of highly confined 2D polaritons. In this section, several near-field optical methods are discussed.

3.1. Scanning Near-Field Optical Microscopy

3.1.1. The Mechanism of SNOM

SNOM was proposed by Synge in 1928 and was first realized by placing a metal film with a small aperture very close to the sample. Light passing through the sub-wavelength diameter aperture provides super-resolution information when the hole-sample distance is far smaller than the wavelength. Based on this principle, aperture SNOM using pointed optical fiber as the scanning probe was developed. The optical fiber can be used as the nanoscale source or detector. Aperture SNOM relies on the light direction and works in either illumination mode (light coming from the aperture) or collection mode (light passing to the aperture). Since the fiber aperture is smaller than the wavelength of the outgoing light, only evanescent waves come through and even out from the probe in illumination mode.

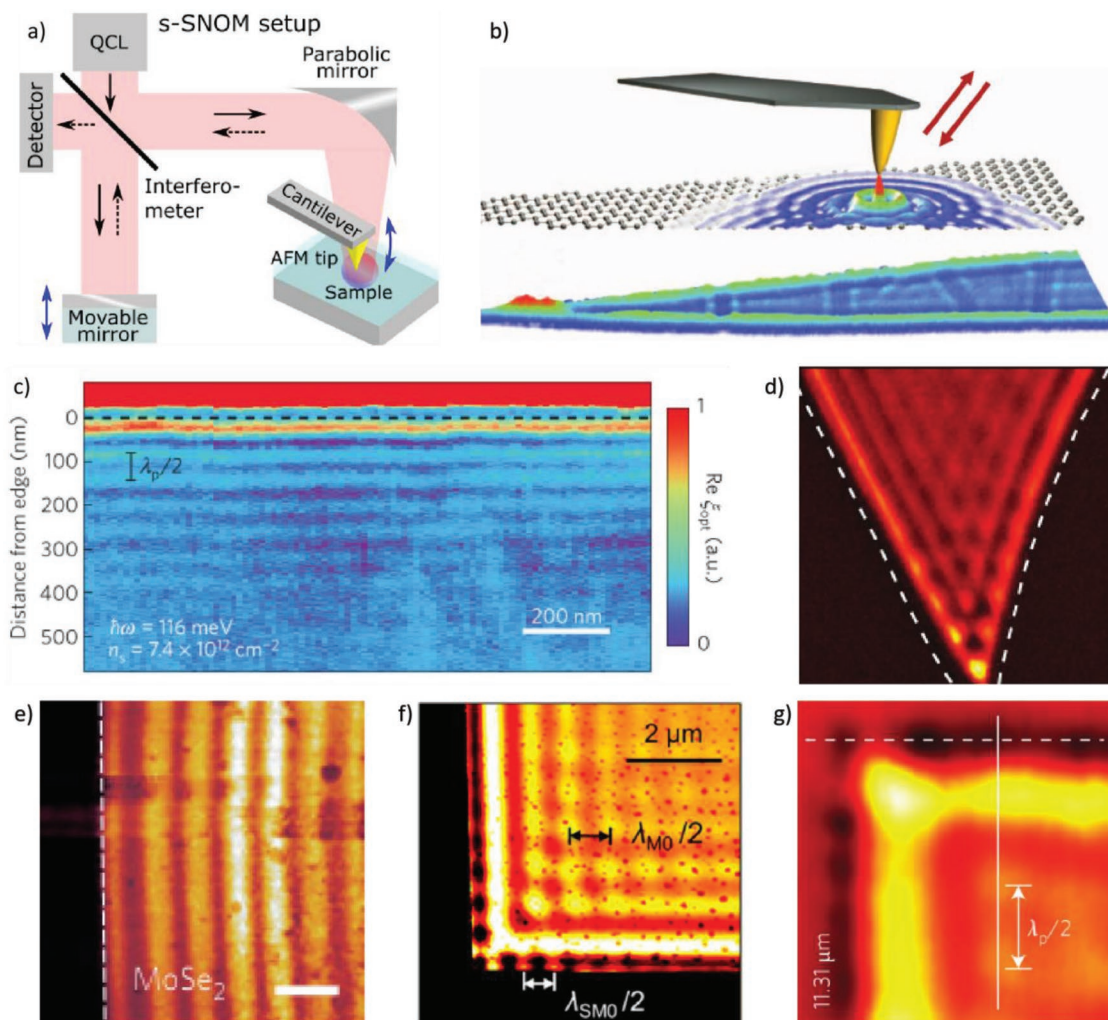


Figure 4. a) Simplified schematic of the s-SNOM setup. The sample is illuminated by a QCL continuous-wave laser through a Michelson interferometer. An AFM tip is tapping on the sample and scatters back light. A moving mirror, oscillating with the same frequency as the tip, is used to demodulate (pseudoheterodyne demodulation) phase and amplitude of the scattered field. Reproduced with permission under the terms of a Creative Commons license 4.0 (CC BY-NC).^[32] Copyright 2018, The Authors, published by American Association for the Advancement of Science (AAAS). b) Imaging propagating and localized graphene plasmons by s-SNOM. Top: Diagram of the experimental configuration used to launch and detect propagating surface waves in graphene. Bottom: Near-field amplitude image acquired for a tapered graphene ribbon on top of 6H-SiC. Reproduced with permission.^[96] Copyright 2012, Springer Nature. c) The s-SNOM optical signal from a 2D scan of the tip position, near the graphene edge (dashed line) at room temperature. Edge-reflected plasmons appear as interference fringes. Reproduced with permission.^[8] Copyright 2014, Springer Nature. d) Phonon polaritons probed in the h-BN crystals. Reproduced with permission.^[97] Copyright 2014, AAAS. e) Near-field amplitude images of MoSe₂ taken at E = 1.38 eV in the perpendicular configuration. Reproduced with permission.^[98] Copyright 2017, Springer Nature. f) Near-field imaging of HPs and HSPs of a 40 nm thick h-BN flake. Reproduced with permission.^[100] Copyright 2017, American Chemical Society. g) The edge graphene plasmons in a large graphene structure on SiO₂ substrate. Reproduced with permission.^[101] Copyright 2016, Springer Nature.

The resolution of aperture SNOM can be hundreds of times lower than the light wavelength and, therefore, offers unique advantages related to visible or ultraviolet illumination. However, the complex fabrication of the aperture and waveguide cut-off effect^[92] make this method difficult and less valuable in practical nanoscience applications.

The SNOM technique based on tip scattering (i.e., s-SNOM) appeared in the late 1990s. Unlike aperture SNOM, s-SNOM typically works using a laser beam focused onto a metalized atomic force microscopy (AFM) probe at an oblique angle of incidence. The resolution of s-SNOM is free from the restriction of the wavelength of the incident light, which is set by the tip radius of the scanning probe (≈ 15 nm). With proper light

sources, s-SNOM can be applied over a broad wavelength range from UV to THz, making s-SNOM powerful and the most widely used near-field optical technique.

Figure 4a^[32] presents a sketch of s-SNOM. The AFM tip is used to enhance and probe the local electric field in close proximity to the sample, which helps to match the light momentum with the sample and enables momentum-resolved optical characterization.^[93] The metallic tip scatters light according to its polarizability under an external light source with a selected frequency. The polarizability of the tip is affected by the dielectric function of the sample at the very vicinity under the tip, where the dielectric function reflects the electronic, vibrational, or phonon resonances of the sample. How to interpret

the collected near-field information is a major challenge because problems like nontrivial tip-sample interactions and undesired signals from background are hard to be completely avoid.^[94] Therefore, sophisticated equipment is needed to decode the collected information. Usually, both the amplitude and phase of the scattered light can be measured by scanning the probe over the sample in tapping mode. Based on the scattering light signal, it is possible to form an image of the polaritons and the dispersion and propagation can be further deduced from the obtained signal.

3.1.2. *s*-SNOM Probing with a Continuous Wave Laser

The most commonly used near-field optical technique is *s*-SNOM working with monochromatic continuous wave light sources. When illuminated with a laser at a certain wavelength, a cylindrical polariton wave is launched by the tip and propagates above the sample surface with wavelength λ_p . When the tip is close enough to the sample boundary, a periodic standing wave with wavelength $\lambda_p/2$ will be formed as a result of interference between the tip-launched polariton wave and the boundary-reflected wave.^[8,95] In this manner, *s*-SNOM can perform direct real-space imaging of polaritonic waves propagating on the surface of the sample.

s-SNOM has been widely used to study different types of ultra-confined 2D polaritons, including plasmons, phonon polaritons, and exciton polaritons. For example, Woessner et al.^[8] and Chen et al.^[96] measured propagating graphene plasmons in real space in 2012, as shown in Figure 4b,c, respectively. The highly compressed wavelength, as well as the dispersion and plasmon damping, can be obtained from real-space imaging. With this technique, the patterns from surface phonon polariton interference on h-BN have also been reported (Figure 4d).^[97] Ma et al.^[27] demonstrated anisotropic phonon polariton propagation for MoO₃. Hu et al.^[98] visualized exciton polaritons in MoSe₂ with apparent fringes (Figure 4e). From the interference patterns, important polariton properties, such as dispersion and propagation loss, can be inferred. Moreover, the waveguide modes in ultrathin 2D materials can also be revealed with *s*-SNOM. Hu et al.^[99] observed excited polaritons in MoS₂, they analyzed the interference patterns, and inferred the anisotropic dielectric function of the material.

Imaging with *s*-SNOM also contributes to a precise knowledge of different resonance modes and efficient devices design. In 2016, Li et al.^[100] revealed the fundamental hyperbolic surface polariton mode at the edges of a thin h-BN flake exhibits a shorter wavelength, smaller group velocities, and nearly identical lifetimes, as compared to the fundamental volume-confined hyperbolic polariton modes of the same h-BN flake (Figure 4f). Within the same year, Nikitin et al.^[101] revealed edge modes at the brim of graphene nanoresonators show higher confinement than sheet plasmons (Figure 4g).

3.1.3. *s*-SNOM-Based Nano-FTIR

The *s*-SNOM-based FTIR technique (nano-FTIR) is also known as broadband nanospectroscopy. In this technique, *s*-SNOM works with a broadband radiation source and the detected

signals are subsequently processed by Fourier transformation. Nano-FTIR delivers point-by-point spectral information over a broad bandwidth (200–5000 cm⁻¹) with ultra-high space resolution. The resolution is about 15 nm (defined by the tip radius), which is dramatically enhanced compared to that of traditional FTIR (about micrometer scale). Nano-FTIR shows great promise in a range of applications involving detection of chemical signals on a nanometer scale, which is of vital importance in today's bio-technology and health-care industries.^[102] This technique has undergone great progress in detecting chemical signals in fine structures in recent years.^[103–106]

For polariton probing, nano-FTIR combines the advantages of both *s*-SNOM and IR spectroscopy, i.e., high space resolution and abundant spectrum information. Nano-FTIR yields a more comprehensive map of polaritons by providing the evolution of the fringe patterns with the frequency and space. Various polaritons have been investigated with nano-FTIR. Alfaro-Mozazwe et al.^[107] clearly distinguished the first six longitudinal resonances in rectangular h-BN waveguide antennas with nano-FTIR, where sharp resonances were observed with large quality factors around 100, which is very different from conventional linear antennas (Figure 5a). Shi et al.^[108] imaged phonon polaritons in h-BN using nano-FTIR based on broadband mid-IR synchrotron radiation, where both amplitude- and phase-resolved spectra were obtained. Moreover, the large spectral bandwidth enables the simultaneous measurement of both out-of-plane (780 cm⁻¹) and in-plane (1370 cm⁻¹) h-BN phonon modes. Dai et al.^[97] determined a series of resonances in different places (Figure 5b). Ma et al.^[27] used nano-FTIR studied anisotropic polaritons in the in-plane anisotropic material MoO₃ with a series of signal maxima shown in two spectral bands, which were obtained along two different in-plane crystal directions (Figure 5c). Based on nano-FTIR, Fei et al.^[109] investigated confined plasmon modes inside patterned graphene nanoribbons and uncovered the evolution of plasmon fringe patterns in graphene with radiation frequency.

3.1.4. Ultrafast *s*-SNOM

Ultrafast *s*-SNOM integrates *s*-SNOM with ultrafast light sources. Ultrafast spectroscopy can perturbatively excite materials on time scales shorter than the underlying correlation dynamics and monitor subsequent temporal evolution. The combination of *s*-SNOM and ultrafast spectroscopy makes it possible to explore the ultrafast dynamics of fundamental excitations with high spatial resolution.^[110]

Many pump-probe techniques have been integrated with *s*-SNOM and yielded spectral coverages ranging from the THz to extreme UV. Figure 5d is a schematic of a typical ultrafast *s*-SNOM, where the femtosecond pump-probe is adopted to drive a nonequilibrium excitation in the sample. The tip-scattering pulses detect the induced polarization density distribution $P(t, r)$ and its evolution in space and time and localized response function $R(t, \tau)$ can be collected by the detector for each sample position. By varying the probe pulse time delay, the response function can be reconstructed.^[110]

In 2014, Wagner et al.^[111] studied the evolution of the area-dependent near-field signals of graphene plasmon and revealed

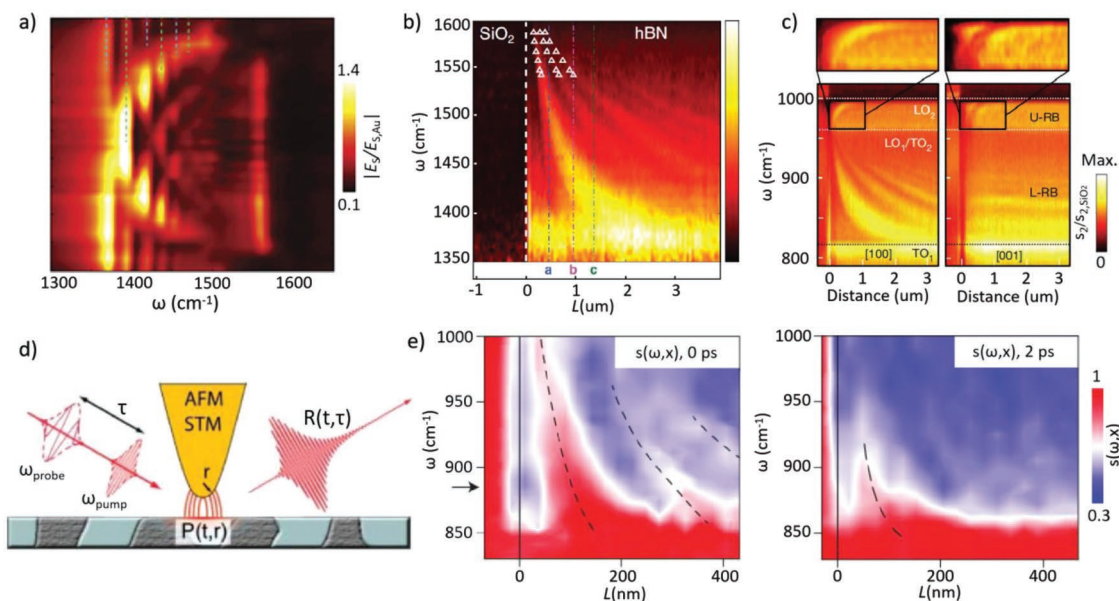


Figure 5. a) Nano-FTIR study of a 1723 nm long linear h-BN antenna on SiO₂. Reproduced with permission.^[107] Copyright 2017, Springer Nature. b) Schematics of a nano-FTIR line scan across the h-BN crystal. Arrows denote the incident and back-scattered infrared beam spanning 1350 to 1600 cm⁻¹. Reproduced with permission.^[97] Copyright 2014, AAAS. c) Nano-FTIR spectral line scans along [100] and [001] showing the near-field amplitude s_2 as a function of distance between tip and the flake edge. Reproduced with permission.^[27] Copyright 2018, Springer Nature. d) Concept of spatio-temporal s-SNOM implementing femtosecond pump-probe schemes for ultrafast spectroscopic nano-imaging. The local read out of the induced spatio-temporal optical polarization distribution $P(t, r)$ via the radiating polarization response $R(t, \tau)$ provides insight into the ultrafast relaxation at each scan point. Reproduced with permission.^[110] Copyright 2012, Taylor & Francis. e) Pump-probe $s(\omega, x)$ data revealing the dispersion of photo-induced plasmons for different pump-probe time delays. These data are displayed in the form of 2D hyperspectral maps of the scattering amplitude $s(\omega, x)$. Reproduced with permission.^[112] Copyright 2016, Springer Nature.

the plasmonic response in graphene was enhanced due to the increase in effective temperature following photoexcitation. In 2016, Ni et al.^[112] activated graphene plasmons with femtosecond optical pulses and delineated the properties of non-equilibrium photo-induced plasmons in a high-mobility graphene monolayer (Figure 5e). Then Huber et al.^[25] realized high-contrast interband excitation of electron-hole pairs in BP using ultrashort near-infrared pulses in a SiO₂/BP/SiO₂ heterostructure. They traced the surface phonon modes of the SiO₂ layers hybridized with surface plasmon modes and found the surface mode could be generated within ≈ 50 fs and disappear within 5 ps. This demonstrates BP is a potential candidate for ultrafast nanophotonic devices.

3.1.5. The Extended Functions of s-SNOM

The optical response in s-SNOM is unperturbed by large magnetic fields, electric fields, current, temperature, and gas pressure, rendering s-SNOM compatible within a range of these conditions.^[110,113] Changes in these factors, especially into extreme conditions with the help of special equipment, is of scientific importance for understanding the fundamental properties of polaritons. The extended functions of s-SNOM in electrical measurements, cryogenic environments, and high-strength magnetic fields are discussed below.

s-SNOM-Based Optoelectronic Nanoscopy: Combining s-SNOM with an electrical read-out allows photocurrent mapping at nanometer resolution. Figure 6a shows a representative schematic of photocurrent nanoscopy detection of the

photocurrent from grain boundaries in graphene. The working principle is a locally concentrated optical field is generated by a mid-infrared laser at the metal tip, which triggers a position-dependent photocurrent in graphene, and the photocurrent is subsequently measured in situ via the contacted electrodes.^[114] The near-field contribution to the total photocurrent can be isolated by oscillating the tip vertically, which is similar to the deduction of background signal for s-SNOM.^[114,115]

Optoelectronic nanoscopy has been demonstrated to detect plasmons electrically. In 2016, Lundeberg et al.^[116] detected the propagating graphene plasmons electrically for the first time. Graphene also acts as a thermoelectric detector by transferring electronic heat into a voltage signal, where a graphene sheet was clipped in h-BN and two separated local gates were fabricated directly underneath the hBN. The electric field implemented by the two gates enables the charge carrier density and polarity to be spatially tunable across the device. Figure 6b is a photocurrent map with interference fringes collected by thermoelectric nanoscopy near the edge of the graphene. In 2017, Alonso-González et al.^[115] successfully electrically detected highly confined THz acoustic graphene plasmons with split-gate architecture. P-n junctions are formed in the graphene near where the gates split. Photocurrent imaging was performed with photocurrent nanoscopy, which revealed photocurrent oscillations near the p-n junction and THz graphene plasmons. This process resembles s-SNOM imaging of infrared graphene plasmons. THz optoelectrical nanoscopy was used to detect the nonlocal response of graphene electron liquid with ultra-slow (at velocities close to the electron Fermi velocity) graphene plasmons, as shown in Figure 6c.^[117]

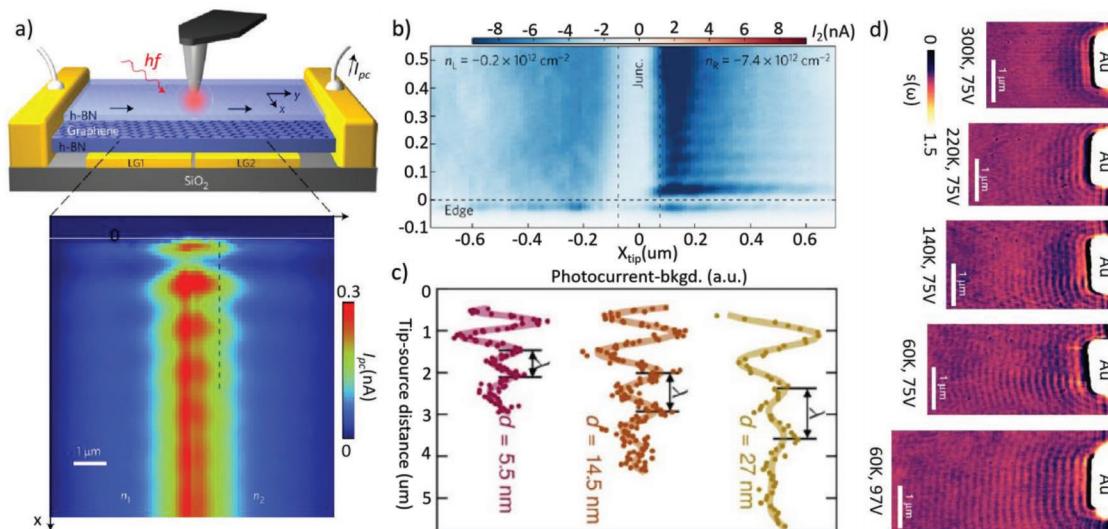


Figure 6. a) Real-space imaging of acoustic THz plasmons in a graphene photodetector with split-gate architecture. Reproduced with permission.^[115] Copyright 2016, Springer Nature. b) High-resolution photocurrent map near the graphene edge, containing interference fringes. Reproduced with permission.^[116] Copyright 2016, Springer Nature. c) Nonlocal response of graphene electron liquid with graphene plasmons under electric fields. Reproduced with permission.^[117] Copyright 2017, The Authors, published by AAAS. d) Nanoscale infrared images of graphene plasmon polaritons acquired at different temperatures and gate voltages. Reproduced with permission.^[120] Copyright 2018, Springer Nature.

Cryogenic s-SNOM: Cryogenic s-SNOM is useful for studying the underlying mechanisms of strongly correlated electron systems and electron–phonon interactions by performing nanometer resolution optical spectroscopy at low temperatures. In 2013, Yang et al. developed a s-SNOM instrument that works at relatively low temperatures and studied domain formation associated with metal–insulator transition of VO₂ ($T_{\text{MIT}} \approx 340$ K) and V₂O₃ ($T_{\text{MIT}} \approx 150$ K).^[113] Then, low-temperature s-SNOM was used to study low-temperature phase transitions in strongly correlated materials by both temperature-dependent resonance spectroscopy and domain distribution imaging.^[118,119]

For polariton characterization, a direct and glaring advantage of cryogenic s-SNOM is that the low temperature largely reduces the damping of polaritons, which has been the main hinderance in the field. In 2018, Ni et al.^[120] investigated propagating plasmon polaritons in high-mobility encapsulated graphene at cryogenic temperatures with s-SNOM. At liquid-nitrogen temperature, the propagation length of the graphene plasmon reached a record high of ≈ 10 μm , which is about 50 times the plasmonic wavelength (Figure 6d). Previously, a long lifetime and propagation distance were notoriously difficult to obtain because polaritons are in highly confined modes in 2D materials. This endeavor revealed dissipation in graphene at low temperatures is due to the surroundings rather than electron scattering in graphene. Cryogenic s-SNOM has great potential for use in studies of the excitations and dynamics of the phases of superconductors, ferromagnets, and antiferromagnets. These phases manifest only at low temperatures and are easily accessible due to being exposed on the surface of 2D materials.^[118,121]

s-SNOM in Magnetic Fields: Magnetic fields are a basic research tool in material science and the use of s-SNOM in strong magnetic fields would be another exciting method of probing polaritons in 2D materials and magnetic samples that would likely yield unique phenomena. However, very limited attempts working with magnetic fields with scanning force

microscope have been conducted to date,^[122] and this method requires further exploration.

Besides s-SNOM, several near-field methods based on AFM with high spatial resolution and broadband spectra have been developed in recent years. Among these, PTIR, PFIR, and PiFM are three examples.

3.2. Photothermal-Induced Resonance Microscopy and Peak Force Infrared Microscopy

PTIR microscopy combines AFM and absorption spectroscopy. PTIR works by detecting near-field absorption rather than scattering and provides nanoscale resolution imaging and spectroscopy over the entire mid-IR spectral range. **Figure 7a** presents a schematic diagram of PTIR.^[123] During this process, the AFM tip is in contact with the sample and, when the sample absorbs the laser pulse energy, there is local thermal expansion of the sample, which induces mechanical motion of the cantilever that can be sensed by an AFM position-sensitive detector system and converted into PTIR signal.^[124] Since the amplitude of the PTIR signal is proportional to the energy absorption, PTIR spectra have been used to map various chemical^[125] and optoelectronics signals.^[29,126,127]

PTIR can be a complementary technique to s-SNOM owing to their different working mechanisms. The former measures absorbed light, while the latter detects scattered light. PTIR and s-SNOM have distinct advantages in probing polaritons related to their two different mechanisms. For example, the bright-modes of plasmon exhibit strong scattering but limited absorption, which is suitable for s-SNOM probing.^[27,96,109,128–131] Meanwhile, the dark (higher order) modes exhibit strong absorption and weak scattering that are suitable for PTIR. PTIR enables the observation of dark modes regardless of the weakness of the weak far-field emission.^[29,132] Recently, Brown et al.^[29]

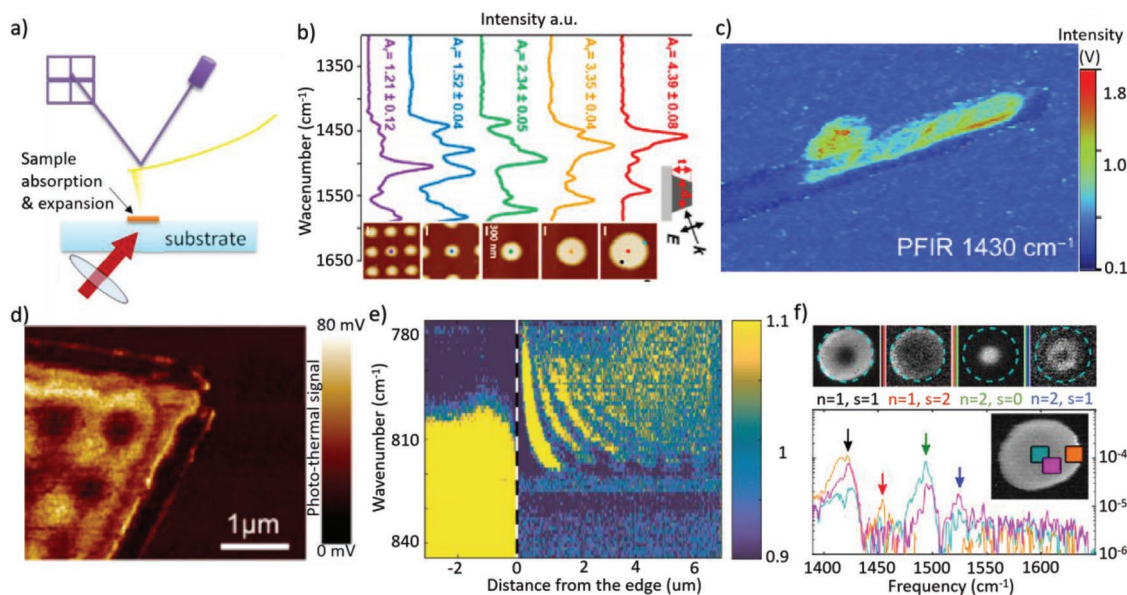


Figure 7. a) Schematic of setup for photo-induced thermal expansion microscopy. The sample under the AFM tip absorbs the laser pulse energy and induces mechanical motion of the AFM cantilever, which is subsequently sensed by an AFM position-sensitive detector system. Reproduced with permission.^[123] Copyright 2011, The Optical Society. b) PTIR absorption spectra (p-polarization) obtained by positioning the AFM tip at the center of h-BN frustums. Reproduced with permission.^[29] Copyright 2018, American Chemical Society (ACS). c) The PFIR image of a boron nitride nanotube at the infrared frequency of 1430 cm^{-1} . Reproduced with permission.^[30] Copyright 2017, The Authors, published by AAAS. d) Zoomed-in photothermal image of one of the corners in the flake obtained by a high mechanical sensitivity AFM cantilever. The illuminating light has a wavenumber of 1440 cm^{-1} . Reproduced with permission.^[133] Copyright 2017, ACS. e) The PiFM signal intensity of h-BN as a function of the distance from the edge and the illuminating light frequency. Reproduced with permission.^[33] Copyright 2018, Springer Nature. f) PiFM images (upper) and extinction spectra (lower) of h-BN nanodiscs. Four resonance modes are detected. From the same hyperspectral measurement, spectra can be obtained in various points on the disc, confirming the resonant wavelength of the modes in discs can be several tens of times smaller than the free space wavelength (about $7\text{ }\mu\text{m}$). Reproduced with permission under the terms of a Creative Commons license 4.0 (CC BY-NC).^[32] Copyright 2018, The Authors, published by AAAS.

detected phonon polaritons in h-BN nanostructures using PTIR (Figure 7b) and directly observed dark hyperbolic modes that had been previously unobserved by other near-field techniques.

PFIR microscopy, which is based on light-induced thermal expansion, was also developed. Distinct from PTIR microscopy, the AFM of PFIR is operated in peak force tapping mode during which the laser pulses (irradiating onto the sample and not) synchronize in every cycle. The cantilever deflection caused by the thermal expansion maintains the same pace and the laser irradiating cycle is traced by the position sensor. Excitation of the contact resonance of the cantilever occurs if the volume expansion is sufficiently rapid. Wang et al.^[30] verified the presence of surface phonon polaritons in boron nitride nanotubes using PFIR microscopy (Figure 7c). In addition, the edges of twisting polygonal facets of boron nitride nanotubes were detected, which s-SNOM is incapable of resolving.

A similar technique that relies on the high mechanical sensitivity of AFM has been also developed, which was used in 2017 by Ambrosio et al.^[133] to realize photonless detection of phonon polaritons for the first time. For this technique, the AFM tip is in contact with h-BN and the lattice vibration of h-BN is enhanced by launched phonon polaritons and is then detected by AFM. In the work by Ambrosio et al., a resolution comparable to the optimal resolution of s-SNOM was achieved (Figure 7d).

In comparison to s-SNOM, PTIR and PFIR are free from optical interferometric detection but rely on the thermal expansion of materials. The signal detected in these techniques arises from the infrared absorption and can allow both chemical

imaging and nanoscale point spectroscopy with one simple laser source with negligible background signal. This is superior to s-SNOM, which usually requires several separate narrow-band or broadband laser sources and has a non-negligible background signal. In particular, PFIR has a higher spatial resolution ($\approx 10\text{ nm}$), which is determined by the contact area of the tapping AFM cantilever with the sample, and it is suitable for probing samples with rough or sticky surfaces. Another advantage of PFIR and PTIR microscopy is their low average power requirements. For example, in work by Wang et al.,^[30] only $20\text{ }\mu\text{W}$ of power was used for a peak force tapping rate of 2 kHz with negligible damage to the sample. In comparison, s-SNOM requires an average of milliwatt levels of power, which may hurt the sample during imaging and spectroscopy. However, the PTIR and PFIR techniques require the sample under investigation to have a thickness comparable to the field penetration depth due to light absorption-thermal expansion, which is not necessary for s-SNOM. In addition, s-SNOM provides 2D scanning images of the sample from which both phase and complex refractive indexes can be deduced, while PTIR and PFIR only provide absorption-dependent spectra.^[30,134]

3.3. Photo-Induced Force Microscopy

PiFM works via the dipole-dipole force interactions between an AFM tip and optically excited sample when the tip gets very close to the sample surface. PiFM operates in tapping mode

at one mechanical resonance of the cantilever and detects the motion of the cantilever at another mechanical resonance. When the energy of the external laser exciting the sample coincides with the energy difference between these two resonances, the sample and tip dipoles interaction will be strongest.^[30] The force interaction in the form of force gradient can be used to detect sample polarizability without detecting any light.

PiFM has been used to visualize molecules on the nanoscale.^[135,136] PiFM can also aid in the detection of 2D polaritons. PiFM images the z component of the field, which has the same distribution of the local charge density due to Gauss's law. This makes hyperspectral image acquisition possible and for more polaritons resonant modes to be captured with a single scan. As shown in Figure 7e, PiFM can effectively map the modes in the lower Reststrahlen band of h-BN that cannot be obtained by s-SNOM due to the lack of continuous wave laser sources.^[32] Ambrosio et al.^[33] selectively excited h-BN with the more confined modes in the lower and upper Reststrahlen bands by PiFM. Figure 7f is a plot of the PiFM signal intensity from h-BN showing the fringe periodicity as a function of the illuminating light wavelength, from which the first mode in the lower Reststrahlen band can be inferred. In addition, Liu et al.^[31] imaged propagating plasmons in graphene by illuminating a mid-infrared laser beam on graphene suspended over a metallic grating with a dielectric spacer. Here, the magnitude of the optical force is proportional to the field intensity of the graphene.

PiFM is a unique AFM-based IR technique that not only excites, but also detects, the sample with near-field, which is a major advantage over s-SNOM due to eliminating the convolution of the topography and electromagnetic interactions of materials visualized.^[30,137] Compared with photothermal techniques, the noncontact tapping mode of the PiFM AFM tip avoids tip-sample interactions, which enable the technique with higher spatial resolution (sub-10 nm), better signal quality, and lower energy consumption.^[138] However, minor limitations for PiFM still exist, including difficulty in obtaining an AFM probe with two mechanical resonances and a suitable frequency difference.

3.4. A Summary of Near-field Optical Methods

In this section, several near-field optical techniques based on probes have been presented. With these near-field optical techniques, propagating polaritons can be visualized directly in real space. Of these, s-SNOM is the most developed and regularly utilized in detecting 2D polaritons. Different light sources and equipment have been fitted to s-SNOM to observe polaritons in terms of space, time, temperature, and electromagnetic field domain. The high spatial resolution, ultrafast pulses, and cryogenic and electromagnetic field environment provide insight into polaritons for full material systems ranging from semimetal to insulator. PTIR, PFIR, and PiFM are other recently developed techniques that focus on detecting light-induced mechanical responses from polaritons. Compared with s-SNOM, their advantages include either a higher spatial resolution, neglectable background signal, or lower energy consumption. However, their application in probing polaritons is still in infancy and under investigation.

4. Electronic Excitation

Compared with optical methods, electronic excitation can supply much larger wavevector matching with the aid of microscopy equipment, which is important for the excitation of highly confined 2D polaritons requiring large wavevector compensation. Moreover, a beam of fast electrons can be focused to nanoscale dimensions (<1 nm) and provides atomic spatial resolution as a result of the de Broglie equation $h = \lambda p$, where p is the momentum of moving electrons, h is Planck constant, and λ is the wavelength of the electronic wave. Free electrons can also generate 2D polaritons in a smaller energy range in the absence of microscopy equipment. In this part, several electron microscope methods, including EELS, CL, PEEM, and PINEM are presented for use in probing 2D polaritons.

4.1. Electron Energy Loss Spectroscopy

EELS is a spectral analysis technique related to energy loss events of transmitted electrons.^[139] Figure 8a^[140] presents the typical structure of EELS, where an electron beam is emitted from an electron gun incident and interact with atoms of the specimen. These interactions can be divided into elastic and inelastic processes depending on whether a considerable energy exchange happens. The inelastic process results in a high zero energy loss peak (ZLP), where the full width at half maximum reflects the energy distribution of the electron source and is associated with the energy resolution. The inelastic scattering results in energy loss peaks due to the excitation of phonons, polaritons, or electrons. As depicted in Figure 8b,^[141] peaks in the low-loss region, typically up to 50 eV, arise from interactions with conduction or valence electrons, where localized surface plasmon resonances and bandgap excitation occur. The high-loss region (>50 eV) is where inelastic scattering with inner-shell electrons happens.

EELS combined with transmission electron microscopy (EELS-TEM) can provide complete information on polariton modes at an improved spatial resolution down to 0.1 nm and energy resolution down to 0.1 eV.^[142] The improvement of the energy resolution can extend the detectable modes from the infrared to the visible-ultraviolet. EELS-TEM has been widely used to excite ultraviolet plasmonic modes in various traditional 2D materials, such as high energy plasmon in graphene,^[34,143–146] black phosphorous,^[147] topological insulators,^[37,148] a recently discovered new class of 2D crystals-MXenes,^[39,149] and the bandgap excitation in h-BN.^[36,150] For example, Eberlein and co-workers^[34] observed π and $\pi + \sigma$ -surface plasmon modes in a few layers of free-standing graphene sheets, where the EEL spectra is shown in Figure 8c. Liou et al.^[148] investigated Bi₂Se₃ single crystals with EELS-TEM and found both volume and surface plasmons (Figure 8d). El-Demellawi et al.^[39] investigated the spatial and energy distribution of plasmon polaritons in mono- and multilayered Ti₃C₂T_x flakes with the help of EELS-TEM (Figure 8e). In addition, both plasmons and excitons modes in MoS₂ can be excited with the aid of EELS-TEM.^[38]

Notably, most of the plasmon modes presented above are located in the ultraviolet region of the electromagnetic

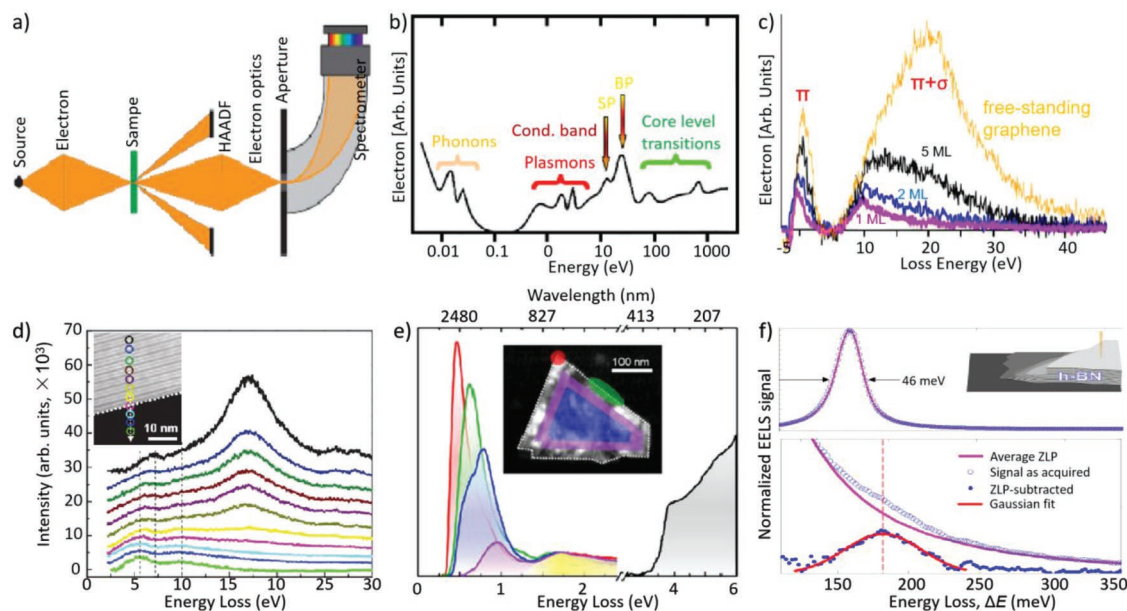


Figure 8. a) Conceptual sketch of EELS measurements in the SPIM configuration. The nanometer-sized electron beam in a STEM is raster-scanned across the sample, and the energy distribution of the transmitted electrons is recorded for each beam position using an EELS spectrometer. Reproduced with permission.^[140] Copyright 2017, Higher Education Press and Springer-Verlag Berlin Heidelberg. b) Regions of characteristic losses. Reproduced with permission.^[141] Copyright 2014, Elsevier Ltd. c) EEL spectra of several layers of graphene showing the π and the $\pi + \sigma$ plasmon. Reproduced with permission.^[34] Copyright 2008, APS. d) STEM-EELS spectra of topological insulator-single-crystal Bi_2Se_3 with the electron probe positioned at various locations of the material. The π plasmon at 7 eV and $\pi + \sigma$ plasmon at 17 eV are volume plasmons and the plasmons at ≈ 5.5 and 10 eV are surface plasmons. Inset: high-angle annular dark field (HAADF) image of Bi_2Se_3 ; probe step, 2 nm. Reproduced with permission.^[148] Copyright 2013, APS. e) ZLP-subtracted EELS of $\text{Ti}_3\text{C}_2\text{T}_x$ flake. Inset: TEM-HAADF micrograph of the $\text{Ti}_3\text{C}_2\text{T}_x$ flake. Reproduced with permission.^[39] Copyright 2018, ACS. f) Typical spectra acquired on h-BN with ZLP width of 46 meV where phonon polariton was probed. Reproduced with permission.^[12] Copyright 2017, Springer Nature.

spectrum, which originates from interband transitions. The study of other polaritons in smaller energy ranges is inhibited by insufficient spectral resolution.^[142] Decreasing the width of ZLP would help overcome this problem. Recently, Govyadinov et al.^[12] narrowed the ZLP width of a conventional EELS-TEM down to below 50 meV and probed phonon polaritons in hBN at a meV energy level (Figure 8f). As high-resolution EELS (HREELS) has an intrinsically smaller energy resolution than EELS-TEM, it is suitable for detecting signals at low energy levels.^[151] However, HREELS is not a commonly used method for polariton characterization in 2D materials due to a lack of high spatial resolution.

4.2. Cathodoluminescence, Photoemission Electron Microscopy, and Photo-Induced Near-Field Electron Microscopy

Polaritons excited by fast electron beams can be dissipated either nonradiatively via energy absorption or radiatively. For the latter, a CL spectral analytical system can be used to capture emitted photons and decode information from the polaritons carried by these photons.^[140] For example, during electron excitation, the moving electrons traveling faster than the phase velocity of the triggered polaritons give rise to direct transformation of plasmon polaritons into radiation (also called Cherenkov radiation), which still widely exists in 2D materials like graphene.^[152–155] CL affords a spatial resolution on the order of 1 nm and the radial extent of the evanescent electric field about the electron beam is on the order of 10 nm. However,

as the spectral extent of excitation is typically less than one femtosecond, the moving electron mainly acts as a ultraviolet/visible optical excitation source.^[156] Moreover, a lacking of efficient optical spectrometers and detectors in the infrared spectral range limits the application of CL. To date, CL emission has only been used to excite polaritons in metallic nanostructures,^[157–159] semiconductors,^[160,161] topological insulator,^[162] or dielectrics.^[163] Extending the detection wavelength down to the mid-infrared range and concurrently protecting 2D materials properly will reap a great deal of new optical phenomena on a wide range of 2D materials such as graphene and boron nitride.

This is also true for PEEM and PINEM. PEEM is a probe-free nonscanning technique implemented based upon the photoelectric effect-ruled photoemission of electrons from a laser-excited sample (also known as photoelectrons). Incident photons with properly low energy can generate (multiple) plasmonic modes via light absorption and a photoelectron will be ejected when these plasmonic modes interact with another incident photon or photoexcited plasmon and will ultimately be recorded by a CCD camera. PEEM is suitable for investigating nonlinear photoemissions and can help characterize the plasmonic properties of the sample.^[140,164] While the resolution of PEEM as an electron microscope is limited by electron optics, this method provides a new approach for dynamically probing polaritons with the desired high spatial and temporal resolution if an ultrafast optical pulse is introduced. However, PEEM currently can only operate in the X-ray spectra to near infrared range and plasmon polaritons have been only investigated on metal films^[164–167] and nanostructures.^[168]

PINEM is another optical excitation method with possibilities for probing 2D polaritons. Distinct from PEEM, PINEM uses a subsequently incident fast electron beam to probe samples after optical excitation. The fast electrons either absorb the photoexcited plasmon in a photon-assisted electron energy gain process or excite a second plasmon through stimulated electron energy loss, where both processes relate to the photoexcited plasmonic near field. Therefore, analyzing the transmitted electrons is helpful for studying photoexcited polaritons.

4.3. A Summary of Electronic Methods

With high energy to be achieved, electronic probing methods have a significant advantage over other techniques, including ultrahigh spatial resolution and good tunability of electron energy. However, a big problem for these techniques is that detection is typically limited to the eV range, which is too large to probe low-energy excitations like mid-infrared phonons or plasmons. In addition, the high energy of the electron beam may be harmful to samples, particularly 2D materials.^[72,169]

How to handle the contradictoriness of energy poses a big challenge for electronic techniques.

5. Summary and Outlook

In this review, a series of methods of probing polaritons were presented. Diffraction gratings, ATR, and all-optical wave mixing methods aim to overcome the wavevector mismatch problem in far-field optical excitation. Using these methods, plasmon and phonon polaritons can be triggered. Tamm plasmon polaritons are unique entities that can be excited by period Bragg mirror. Subsequently, near-field techniques with high spatial resolutions of about 15 nm, including s-SNOM, PTIR, PFIR, and PiFM, were presented. s-SNOM, a widely used near-field technique with great potential for future applications, was discussed in detail in terms of its utilization with difference light sources and environments. Using near-field techniques, plasmons, excitons, and phonon polaritons can be all excited in different material systems. Finally, electronic probing techniques are covered, larger wavevector mismatch

Table 1. Comparison between far-field optical, near-field optical, and electronic techniques for probing 2D materials polaritons.

	Method	Advantages	Weaknesses	Common places
Far-field optical technique	Diffraction gratings	Easy to handle; Large spectral range (from THz to mid-infrared)	Low spatial resolution; Need large sample area (micrometer scale); Need nanofabrication	Low spatial resolution (micrometer scale); The size of sample is demanded at least up to micrometers scale; Short signal collecting time (≈ 1 min)
	ATR	Free from nanofabrication; Easy to handle with	The direct contact with prism may damage 2D materials and their nanostructures	
	Nonlinear wave mixing	Free from nanofabrication; All-optical	Only suitable for graphene and topological insulator materials; Inefficient; Small tunability range (THz range)	
Near-field optical technique	s-SNOM	High resolution; Visualized	Weak signal strength; Require high quality for the sample; Limited laser source	High resolution (≈ 10 nm); Long signal collecting time (≈ 1 h); Weak signal magnitude; Susceptible to the quality of sample; Not affected by the size of the sample; Fine equipment requirement and complex operation
	PTIR & PFIR	High resolution; Negligible background signal; Detecting higher order mode; Low energy requirement; Visualized	Demand material with thicknesses comparable to the field penetration depth	
	PiFM	High resolution; Independent of film thickness; Negligible background signal; Visualized	Require special probe designs	
Electronic technique	EELS	Suitable for high wavevector polaritons; Ultrahigh spatial resolution (0.1 nm); Wide spectral range (from ultraviolet to infrared)	High energy is not suitable for low energy polaritons and is harmful to 2D materials; Insufficient spectrum range	Ultrahigh spatial resolution (0.1 nm)

can be made up with these setups. Among which, EELS is the major available method used to excite polaritons. Other electronic techniques, such as CL, PEEM, and PINEM, despite lacking examples of detecting polaritons in 2D materials, still hold great potential for future applications. **Table 1** summarizes these techniques, including their pros and cons.

The topic of polaritons in 2D materials is meaningful, but extensive, and thus a challenge to completely cover. This review merely scratches the surface of this subject through the lens of the most commonly seen measurements. To probe polaritons more efficiently, efforts should not be spared. One potential avenue is through combining different techniques according to their characteristics. A good example is combining the broadband spectrum of nano-FTIR with the high resolution of s-SNOM. In addition, exploring new materials with unique polariton phenomena may not only enrich the library of polariton materials, but also provide another force to push characterization techniques to be more powerful.

Acknowledgements

This work was supported by the National Basic Key Research Program of China (grant no. 2015CB932400), the National Key Research and Development Program of China (grant no. 2016YFA0201600), the National Natural Science Foundation of China (grant nos. 11674073, 11504063, 11704085), the key program of the Bureau of Frontier Sciences and Education, Chinese Academy of Sciences (QYZDB-SSW-SLH021), the Key Research Program of the Chinese Academy of Sciences (ZDBS-SSW-JSC002), Youth Innovation Promotion Association CAS, and CAS Interdisciplinary Innovation Team (JCTD-2018-03).

Conflict of Interest

The authors declare no conflict of interest.

Keywords

2D materials, EELS, far-field optical methods, near-field optical methods, polaritons

Received: August 20, 2019

Revised: November 15, 2019

Published online: January 7, 2020

- [1] F. Xia, H. Wang, D. Xiao, M. Dubey, A. Ramasubramaniam, *Nat. Photonics* **2014**, *8*, 899.
- [2] T. Low, A. Chaves, J. D. Caldwell, A. Kumar, N. X. Fang, P. Avouris, T. F. Heinz, F. Guinea, L. Martin-Moreno, F. Koppens, *Nat. Mater.* **2017**, *16*, 182.
- [3] X. Luo, T. Qiu, W. Lu, Z. Ni, *Mater. Sci. Eng. R Rep.* **2013**, *74*, 351.
- [4] E. Ozbay, *Science* **2006**, *311*, 189.
- [5] R. S. Anwar, H. Ning, L. Mao, *Dig. Commun. Netw.* **2018**, *4*, 244.
- [6] W. L. Barnes, A. Dereux, T. W. Ebbesen, *Nature* **2003**, *424*, 824.
- [7] J. D. Caldwell, I. Aharonovich, G. Cassabo, J. H. Edgar, B. Gil, D. N. Basov, *Nat. Rev. Mater.* **2019**, *4*, 552.
- [8] A. Woessner, M. B. Lundeberg, Y. Gao, A. Principi, P. Alonso-González, M. Carrega, K. Watanabe, T. Taniguchi, G. Vignale, M. Polini, J. Hone, R. Hillenbrand, F. H. L. Koppens, *Nat. Mater.* **2015**, *14*, 421.
- [9] N. Mauser, A. Hartschuh, *Chem. Soc. Rev.* **2014**, *43*, 1248.
- [10] S. Mastel, M. B. Lundeberg, P. Alonso-Gonzalez, Y. Gao, K. Watanabe, T. Taniguchi, J. Hone, F. H. L. Koppens, A. Y. Nikitin, R. Hillenbrand, *Nano Lett.* **2017**, *17*, 6526.
- [11] Z. Fei, G. O. Andreev, W. Bao, L. M. Zhang, A. S. McLeod, C. Wang, M. K. Stewart, Z. Zhao, G. Dominguez, M. Thiemens, M. M. Fogler, M. J. Tauber, A. H. Castro-Neto, C. N. Lau, F. Keilmann, D. N. Basov, *Nano Lett.* **2011**, *11*, 4701.
- [12] A. A. Goyadinov, A. Konečná, A. Chuvilin, S. Vélez, I. Dolado, A. Y. Nikitin, S. Lopatin, F. Casanova, L. E. Hueso, J. Aizpurua, R. Hillenbrand, *Nat. Commun.* **2017**, *8*, 95.
- [13] R. F. Egerton, *Rep. Prog. Phys.* **2009**, *72*, 016502.
- [14] F. J. Garcia de Abajo, *ACS Photonics* **2014**, *1*, 135.
- [15] M. Autore, P. Li, I. Dolado, F. J. Alfaro-Mozaz, R. Esteban, A. Atxabal, F. Casanova, L. E. Hueso, P. Alonso-Gonzalez, J. Aizpurua, A. Y. Nikitin, S. Velez, R. Hillenbrand, *Light: Sci. Appl.* **2018**, *7*, 17172.
- [16] L. Ju, B. Geng, J. Horng, C. Girit, M. Martin, Z. Hao, H. A. Bechtel, X. Liang, A. Zettl, Y. R. Shen, F. Wang, *Nat. Nanotechnol.* **2011**, *6*, 630.
- [17] P. Di Pietro, M. Ortolani, O. Limaj, A. Di Gaspare, V. Giliberti, F. Giorgianni, M. Brahlek, N. Bansal, N. Koirala, S. Oh, P. Calvani, S. Lupi, *Nat. Nanotechnol.* **2013**, *8*, 556.
- [18] T. G. Folland, T. W. W. Maß, J. R. Matson, J. R. Nolen, S. Liu, K. Watanabe, T. Taniguchi, J. H. Edgar, T. Taubner, J. D. Caldwell, *MRS Commun.* **2018**, *8*, 1418.
- [19] C. How Gan, *Appl. Phys. Lett.* **2012**, *101*, 111609.
- [20] Y. V. Bludov, M. I. Vasilevskiy, N. M. R. Peres, *EPL* **2010**, *92*, 68001.
- [21] T. J. Constant, S. M. Hornett, D. E. Chang, E. Hendry, *Nat. Phys.* **2016**, *12*, 124.
- [22] B. Yao, Y. Liu, S.-W. Huang, C. Choi, Z. Xie, J. Flor Flores, Y. Wu, M. Yu, D.-L. Kwong, Y. Huang, Y. Rao, X. Duan, C. W. Wong, *Nat. Photonics* **2018**, *12*, 22.
- [23] X. Yao, M. Tokman, A. Belyanin, *Phys. Rev. Lett.* **2014**, *112*, 055501.
- [24] Z. Fei, M. E. Scott, D. J. Gosztola, J. J. Foley, J. Yan, D. G. Mandrus, H. Wen, P. Zhou, D. W. Zhang, Y. Sun, J. R. Guest, S. K. Gray, W. Bao, G. P. Wiederrecht, X. Xu, *Phys. Rev. B* **2016**, *94*, 081402.
- [25] M. A. Huber, F. Mooshammer, M. Plankl, L. Viti, F. Sandner, L. Z. Kastner, T. Frank, J. Fabian, M. S. Vitiello, T. L. Cocker, R. Huber, *Nat. Nanotechnol.* **2017**, *12*, 207.
- [26] P. Li, I. Dolado, F. J. Alfaro-Mozaz, F. Casanova, L. E. Hueso, S. Liu, J. H. Edgar, A. Y. Nikitin, S. Vélez, R. Hillenbrand, *Science* **2018**, *359*, 892.
- [27] W. Ma, P. Alonso-Gonzalez, S. Li, A. Y. Nikitin, J. Yuan, J. Martin-Sanchez, J. Taboada-Gutierrez, I. Amenabar, P. Li, S. Velez, C. Tollan, Z. Dai, Y. Zhang, S. Sriram, K. Kalantar-Zadeh, S. T. Lee, R. Hillenbrand, Q. Bao, *Nature* **2018**, *562*, 557.
- [28] J. Yuan, W. Ma, L. Zhang, Y. Lu, M. Zhao, H. Guo, J. Zhao, W. Yu, Y. Zhang, K. Zhang, H. Y. Hoh, X. Li, K. P. Loh, S. Li, C. Qiu, Q. Bao, *ACS Photonics* **2017**, *4*, 3055.
- [29] L. V. Brown, M. Davanco, Z. Sun, A. Kretinin, Y. Chen, J. R. Matson, I. Vurgaftman, N. Sharac, A. J. Giles, M. M. Fogler, T. Taniguchi, K. Watanabe, K. S. Novoselov, S. A. Maier, A. Centrone, J. D. Caldwell, *Nano Lett.* **2018**, *18*, 1628.
- [30] L. Wang, H. Wang, M. Wagner, Y. Yan, D. S. Jakob, X. G. Xu, *Sci. Adv.* **2017**, *3*, e1700255.
- [31] J. Liu, S. Park, D. Nowak, M. Tian, Y. Wu, H. Long, K. Wang, B. Wang, P. Lu, *Laser Photonics Rev.* **2018**, *12*, 1800040.
- [32] M. Tamagnone, A. Ambrosio, K. Chaudhary, L. A. Jauregui, P. Kim, W. L. Wilson, F. Capasso, *Sci. Adv.* **2018**, *4*, eaat7189.
- [33] A. Ambrosio, M. Tamagnone, K. Chaudhary, L. A. Jauregui, P. Kim, W. L. Wilson, F. Capasso, *Light: Sci. Appl.* **2018**, *7*, 27.

- [34] T. Eberlein, U. Bangert, R. R. Nair, R. Jones, M. Gass, A. L. Bleloch, K. S. Novoselov, A. Geim, P. R. Briddon, *Phys. Rev. B* **2008**, *77*, 233406.
- [35] R. J. Wu, M. Topsakal, T. Low, M. C. Robbins, N. Haratipour, J. S. Jeong, R. M. Wentzcovitch, S. J. Koester, K. A. Mkhoyan, *J. Vac. Sci. Technol., A* **2015**, *33*, 060604.
- [36] C. T. Pan, R. R. Nair, U. Bangert, Q. Ramasse, R. Jalil, R. Zan, C. R. Seabourne, A. J. Scott, *Phys. Rev. B* **2012**, *85*, 045440.
- [37] I. A. Nechaev, I. Aguilera, V. De Renzi, A. di Bona, A. L. Rizzini, A. M. Mio, G. Nicotra, A. Politano, S. Scalse, Z. S. Aliev, M. B. Babanly, C. Friedrich, S. Bluegel, E. V. Chulkov, *Phys. Rev. B* **2015**, *91*, 245123.
- [38] H. C. Nerl, K. T. Winther, F. S. Hage, K. S. Thygesen, L. Houben, C. Backes, J. N. Coleman, Q. M. Ramasse, V. Nicolosi, *npj 2D Mater. Appl.* **2017**, *1*, 2.
- [39] J. K. El-Demellawi, S. Lopatin, J. Yin, O. F. Mohammed, H. N. Alshareef, *ACS Nano* **2018**, *12*, 8485.
- [40] Y. Liu, R. F. Willis, K. V. Emtsev, T. Seyller, *Phys. Rev. B* **2008**, *78*, 201403.
- [41] S. J. Elston, G. P. Bryan-Brown, J. R. Sambles, *Phys. Rev. B* **1991**, *44*, 6393.
- [42] R. A. Watts, T. W. Preist, J. R. Sambles, *Phys. Rev. Lett.* **1997**, *79*, 3978.
- [43] V. W. Brar, M. S. Jang, M. Sherrott, J. J. Lopez, H. A. Atwater, *Nano Lett.* **2013**, *13*, 2541.
- [44] H. G. Yan, X. S. Li, B. Chandra, G. Tulevski, Y. Q. Wu, M. Freitag, W. J. Zhu, P. Avouris, F. N. Xia, *Nat. Nanotechnol.* **2012**, *7*, 330.
- [45] H. Yan, T. Low, F. Guinea, F. Xia, P. Avouris, *Nano Lett.* **2014**, *14*, 4581.
- [46] A. V. Zayats, I. I. Smolyaninov, A. A. Maradudin, *Phys. Rep.* **2005**, *408*, 131.
- [47] H. G. Yan, T. Low, W. J. Zhu, Y. Q. Wu, M. Freitag, X. S. Li, F. Guinea, P. Avouris, F. N. Xia, *Nat. Photonics* **2013**, *7*, 394.
- [48] Z. Liu, K. Aydin, *Nano Lett.* **2016**, *16*, 3457.
- [49] W. Gao, G. Shi, Z. Jin, J. Shu, Q. Zhang, R. Vajtai, P. M. Ajayan, J. Kono, Q. Xu, *Nano Lett.* **2013**, *13*, 3698.
- [50] F. J. Alfaro-Mozaz, S. G. Rodrigo, P. Alonso-Gonzalez, S. Velez, I. Dolado, F. Casanova, L. E. Hueso, L. Martin-Moreno, R. Hillenbrand, A. Y. Nikitin, *Nat. Commun.* **2019**, *10*, 42.
- [51] V. W. Brar, M. S. Jang, M. Sherrott, S. Kim, J. J. Lopez, L. B. Kim, M. Choi, H. Atwater, *Nano Lett.* **2014**, *14*, 3876.
- [52] Y. Jia, H. Zhao, Q. Guo, X. Wang, H. Wang, F. Xia, *ACS Photonics* **2015**, *2*, 907.
- [53] X. Yang, F. Zhai, H. Hu, D. Hu, R. Liu, S. Zhang, M. Sun, Z. Sun, J. Chen, Q. Dai, *Adv. Mater.* **2016**, *28*, 2931.
- [54] H. Hu, X. Yang, F. Zhai, D. Hu, R. Liu, K. Liu, Z. Sun, Q. Dai, *Nat. Commun.* **2016**, *7*, 12334.
- [55] Z. Fang, S. Thongrattanasiri, A. Schlather, Z. Liu, L. L. Ma, Y. M. Wang, P. M. Ajayan, P. Nordlander, N. J. Halas, F. J. G. de Abajo, *ACS Nano* **2013**, *7*, 2388.
- [56] H. Yan, Z. Q. Li, X. S. Li, W. J. Zhu, P. Avouris, F. N. Xia, *Nano Lett.* **2012**, *12*, 3766.
- [57] J. D. Caldwell, O. J. Glembocki, Y. Francescato, N. Sharac, V. Giannini, F. J. Bezares, J. P. Long, J. C. Owrutsky, I. Vurgaftman, J. G. Tischler, V. D. Wheeler, N. D. Bassim, L. M. Shirey, R. Kasica, S. A. Maier, *Nano Lett.* **2013**, *13*, 3690.
- [58] I. Rzdolski, Y. Chen, A. J. Giles, S. Gewinner, W. Schollkopf, M. Hong, M. Wolf, V. Giannini, J. D. Caldwell, S. A. Maier, A. Paarmann, *Nano Lett.* **2016**, *16*, 6954.
- [59] I. Chatzakakis, A. Krishna, J. Culbertson, N. Sharac, A. J. Giles, M. G. Spencer, J. D. Caldwell, *Opt. Lett.* **2018**, *43*, 2177.
- [60] J. D. Caldwell, A. V. Kretinin, Y. Chen, V. Giannini, M. M. Fogler, Y. Francescato, C. T. Ellis, J. G. Tischler, C. R. Woods, A. J. Giles, M. Hong, K. Watanabe, T. Taniguchi, S. A. Maier, K. S. Novoselov, *Nat. Commun.* **2014**, *5*, 5221.
- [61] M. P. Fischer, A. Riede, K. Gallacher, J. Frigerio, G. Pellegrini, M. Ortolani, D. J. Paul, G. Isella, A. Leitenstorfer, P. Biagioni, D. Bida, *Light: Sci. Appl.* **2018**, *7*, 106.
- [62] P. Genevet, J. P. Tetienne, E. Gatzogiannis, R. Blanchard, M. A. Kats, M. O. Scully, F. Capasso, *Nano Lett.* **2010**, *10*, 4880.
- [63] B. Weng, J. Qiu, Z. Shi, *Appl. Phys. B* **2017**, *123*, 29.
- [64] D. Wasserman, E. A. Shaner, J. G. Cederberg, *Appl. Phys. Lett.* **2007**, *90*, 191102.
- [65] K. Y. M. Yeung, J. Chee, H. Yoon, Y. Song, J. Kong, D. Ham, *Nano Lett.* **2014**, *14*, 2479.
- [66] S. S. Sunku, G. X. Ni, B. Y. Jiang, H. Yoo, A. Sternbach, A. S. McLeod, T. Stauber, L. Xiong, T. Taniguchi, K. Watanabe, P. Kim, M. M. Fogler, D. N. Basov, *Science* **2018**, *362*, 1153.
- [67] G. Isfort, K. Schierbaum, D. Zerulla, *Phys. Rev. B* **2006**, *74*, 033404.
- [68] S. G. Menabde, D. R. Mason, E. E. Kornev, C. Lee, N. Park, *Sci. Rep.* **2016**, *6*, 21523.
- [69] N. C. Passler, C. R. Gubbin, T. G. Folland, I. Rzdolski, D. S. Katzer, D. F. Storm, M. Wolf, S. De Liberato, J. D. Caldwell, A. Paarmann, *Nano Lett.* **2018**, *18*, 4285.
- [70] E. L. Runnerstrom, K. P. Kelley, T. G. Folland, J. R. Nolen, N. Engheta, J. D. Caldwell, J. P. Maria, *Nano Lett.* **2019**, *19*, 948.
- [71] N. C. Passler, I. Rzdolski, S. Gewinner, W. Schöllkopf, M. Wolf, A. Paarmann, *ACS Photonics* **2017**, *4*, 1048.
- [72] T. G. Folland, L. Nordin, D. Wasserman, J. D. Caldwell, *J. Appl. Phys.* **2019**, *125*, 191102.
- [73] J. D. Cox, F. J. Garcia de Abajo, *ACS Photonics* **2015**, *2*, 306.
- [74] J. W. You, S. R. Bongu, Q. Bao, N. C. Panoui, *Nanophotonics* **2018**, *8*, 63.
- [75] A. Autere, H. Jussila, Y. Dai, Y. Wang, H. Lipsanen, Z. Sun, *Adv. Mater.* **2018**, *30*, 1705963.
- [76] J. D. Cox, I. Silveiro, F. J. Garcia de Abajo, *ACS Nano* **2016**, *10*, 1995.
- [77] H. A. Hafez, S. Kovalev, J. C. Deinert, Z. Mics, B. Green, N. Awari, M. Chen, S. Germanskiy, U. Lehnert, J. Teichert, Z. Wang, K. J. Tielrooij, Z. Liu, Z. Chen, A. Narita, K. Mullen, M. Bonn, M. Gensch, D. Turchinovich, *Nature* **2018**, *561*, 507.
- [78] Y. Wang, M. Tokman, A. Belyanin, *Phys. Rev. B* **2016**, *94*, 195442.
- [79] J. L. Cheng, N. Vermeulen, J. E. Sipe, *Sci. Rep.* **2017**, *7*, 43843.
- [80] C. J. Tollerton, J. Bohn, T. J. Constant, S. A. R. Horsley, D. E. Chang, E. Hendry, D. Z. Li, *Sci. Rep.* **2019**, *9*, 3267.
- [81] A. V. Kavokin, I. A. Shelykh, G. Malpuech, *Phys. Rev. B* **2005**, *72*, 233102.
- [82] M. Kaliteevski, I. Iorsh, S. Brand, R. A. Abram, J. M. Chamberlain, A. V. Kavokin, I. A. Shelykh, *Phys. Rev. B* **2007**, *76*, 165415.
- [83] K. J. Lee, J. W. Wu, K. Kim, *Opt. Express* **2013**, *21*, 28817.
- [84] C. Symonds, G. Lheureux, J. P. Hugonin, J. J. Greffet, J. Laverdant, G. Brucoli, A. Lemaître, P. Senellart, J. Bellessa, *Nano Lett.* **2013**, *13*, 3179.
- [85] Y. Gong, X. Liu, H. Lu, L. Wang, G. Wang, *Opt. Express* **2011**, *19*, 18393.
- [86] H. Lu, X. Gan, B. Jia, D. Mao, J. Zhao, *Opt. Lett.* **2016**, *41*, 4743.
- [87] L. Wang, M. Bie, W. Cai, X. Zhang, J. Xu, *Phys. Rev. Appl.* **2019**, *12*, 024057.
- [88] K. Zhou, L. Lu, J. Song, B. Li, Q. Cheng, *J. Appl. Phys.* **2018**, *124*, 123102.
- [89] J. Schiefele, J. Pedrós, F. Sols, F. Calle, F. Guinea, *Phys. Rev. Lett.* **2013**, *111*, 237405.
- [90] M. Farhat, S. Guenneau, H. Bağcı, *Phys. Rev. Lett.* **2013**, *111*, 237404.
- [91] L. Novotny, *Prog. Opt.* **2007**, *50*, 137.
- [92] F. Keilmann, R. Hillenbrand, *Philos. Trans. R. Soc. Lond. Ser. A Math., Phys. Eng. Sci.* **2004**, *362*, 787.
- [93] X. Chen, D. Hu, R. Mescall, G. You, D. N. Basov, Q. Dai, M. Liu, *Adv. Mater.* **2019**, 1804774.
- [94] L. Wang, X. G. Xu, *Nat. Commun.* **2015**, *6*, 8973.

- [95] A. M. Dubrovkin, B. Qiang, H. N. S. Krishnamoorthy, N. I. Zheludev, Q. J. Wang, *Nat. Commun.* **2018**, *9*, 1762.
- [96] J. N. Chen, M. Badioli, P. Alonso-Gonzalez, S. Thongrattanasiri, F. Huth, J. Osmond, M. Spasenovic, A. Centeno, A. Pesquera, P. Godignon, A. Z. Elorza, N. Camara, F. J. G. de Abajo, R. Hillenbrand, F. H. L. Koppens, *Nature* **2012**, *487*, 77.
- [97] S. Dai, Z. Fei, Q. Ma, A. S. Rodin, M. Wagner, A. S. McLeod, M. K. Liu, W. Gannett, W. Regan, K. Watanabe, T. Taniguchi, M. Thiemens, G. Dominguez, A. H. C. Neto, A. Zettl, F. Keilmann, P. Jarillo-Herrero, M. M. Fogler, D. N. Basov, *Science* **2014**, *343*, 1125.
- [98] F. Hu, Y. Luan, M. E. Scott, J. Yan, D. G. Mandrus, X. Xu, Z. Fei, *Nat. Photonics* **2017**, *11*, 356.
- [99] D. Hu, X. Yang, C. Li, R. Liu, Z. Yao, H. Hu, S. N. G. Corder, J. Chen, Z. Sun, M. Liu, Q. Dai, *Nat. Commun.* **2017**, *8*, 1471.
- [100] P. Li, I. Dolado, F. J. Alfaro-Mozaz, A. Y. Nikitin, F. Casanova, L. E. Hueso, S. Velez, R. Hillenbrand, *Nano Lett.* **2017**, *17*, 228.
- [101] A. Y. Nikitin, P. Alonso González, S. Vélez, S. Mastel, A. Centeno, A. Pesquera, A. Zurutuza, F. Casanova, L. E. Hueso, F. H. L. Koppens, R. Hillenbrand, *Nat. Photonics* **2016**, *10*, 239.
- [102] E. A. Muller, B. Pollard, M. B. Raschke, *J. Phys. Chem. Lett.* **2015**, *6*, 1275.
- [103] C. Y. Wu, W. J. Wolf, Y. Levartovsky, H. A. Bechtel, M. C. Martin, F. D. Toste, E. Gross, *Nature* **2017**, *541*, 511.
- [104] A. J. Huber, J. Wittborn, R. Hillenbrand, *Nanotechnology* **2010**, *21*, 235702.
- [105] H. A. Bechtel, E. A. Muller, R. L. Olmon, M. C. Martin, M. B. Raschke, *Proc. Natl. Acad. Sci. U.S.A.* **2014**, *111*, 7191.
- [106] F. Huth, A. Goyadinov, S. Amarie, W. Nuansing, F. Keilmann, R. Hillenbrand, *Nano Lett.* **2012**, *12*, 3973.
- [107] F. J. Alfaro-Mozaz, P. Alonso-González, S. Vélez, I. Dolado, M. Autore, S. Mastel, F. Casanova, L. E. Hueso, P. Li, A. Y. Nikitin, R. Hillenbrand, *Nat. Commun.* **2017**, *8*, 15624.
- [108] Z. Shi, H. A. Bechtel, S. Berweger, Y. Sun, B. Zeng, C. Jin, H. Chang, M. C. Martin, M. B. Raschke, F. Wang, *ACS Photonics* **2015**, *2*, 790.
- [109] Z. Fei, M. D. Goldflam, J. S. Wu, S. Dai, M. Wagner, A. S. McLeod, M. K. Liu, K. W. Post, S. Zhu, G. C. A. M. Janssen, M. M. Fogler, D. N. Basov, *Nano Lett.* **2015**, *15*, 8271.
- [110] J. M. Atkin, S. Berweger, A. C. Jones, M. B. Raschke, *Adv. Phys.* **2012**, *61*, 745.
- [111] M. Wagner, Z. Fei, A. S. McLeod, A. S. Rodin, W. Bao, E. G. Iwinski, Z. Zhao, M. Goldflam, M. Liu, G. Dominguez, M. Thiemens, M. M. Fogler, A. H. Castro Neto, C. N. Lau, S. Amarie, F. Keilmann, D. N. Basov, *Nano Lett.* **2014**, *14*, 894.
- [112] G. X. Ni, L. Wang, M. D. Goldflam, M. Wagner, Z. Fei, A. S. McLeod, M. K. Liu, F. Keilmann, B. Özyilmaz, A. H. Castro Neto, J. Hone, M. M. Fogler, D. N. Basov, *Nat. Photonics* **2016**, *10*, 244.
- [113] H. U. Yang, E. Hebestreit, E. E. Josberger, M. B. Raschke, *Rev. Sci. Instrum.* **2013**, *84*, 023701.
- [114] A. Woessner, P. Alonso-Gonzalez, M. B. Lundeberg, Y. Gao, J. E. Barrios-Vargas, G. Navickaite, Q. Ma, D. Janner, K. Watanabe, A. W. Cummings, T. Taniguchi, V. Pruneri, S. Roche, P. Jarillo-Herrero, J. Hone, R. Hillenbrand, F. H. L. Koppens, *Nat. Commun.* **2016**, *7*, 10783.
- [115] P. Alonso-González, A. Y. Nikitin, Y. Gao, A. Woessner, M. B. Lundeberg, A. Principi, N. Forcellini, W. Yan, S. Vélez, A. J. Huber, K. Watanabe, T. Taniguchi, F. Casanova, L. E. Hueso, M. Polini, J. Hone, F. H. L. Koppens, R. Hillenbrand, *Nat. Nanotechnol.* **2017**, *12*, 31.
- [116] M. B. Lundeberg, Y. Gao, A. Woessner, C. Tan, P. Alonso-Gonzalez, K. Watanabe, T. Taniguchi, J. Hone, R. Hillenbrand, F. H. L. Koppens, *Nat. Mater.* **2017**, *16*, 204.
- [117] M. B. Lundeberg, Y. Gao, R. Asgari, C. Tan, B. Van Duppen, M. Autore, P. Alonso-González, A. Woessner, K. Watanabe, T. Taniguchi, R. Hillenbrand, J. Hone, M. Polini, F. H. L. Koppens, *Science* **2017**, *357*, 187.
- [118] H. Hu, X. Yang, X. Guo, K. Khaliji, S. R. Biswas, F. J. Garcia de Abajo, T. Low, Z. Sun, Q. Dai, *Nat. Commun.* **2019**, *10*, 1131.
- [119] A. S. McLeod, E. V. Heumen, J. G. Ramirez, S. Wang, T. Saerbeck, S. Guenon, M. Goldflam, L. Anderegg, P. Kelly, A. Mueller, M. K. Liu, I. K. Schuller, D. N. Basov, *Nat. Phys.* **2017**, *13*, 80.
- [120] G. X. Ni, A. S. McLeod, Z. Sun, L. Wang, L. Xiong, K. W. Post, S. S. Sunku, B. Y. Jiang, J. Hone, C. R. Dean, M. M. Fogler, D. N. Basov, *Nature* **2018**, *557*, 530.
- [121] S. Chakravarty, B. I. Halperin, D. R. Nelson, *Phys. Rev. B* **1989**, *39*, 2344.
- [122] S. Dai, W. Fang, N. Rivera, Y. Stehle, B. Y. Jiang, J. Shen, R. Y. Tay, C. J. Ciccarino, Q. Ma, D. Rodan-Legrain, P. Jarillo-Herrero, E. H. T. Teo, M. M. Fogler, P. Narang, J. Kong, D. N. Basov, *Adv. Mater.* **2019**, *31*, 1806603.
- [123] F. Lu, M. A. Belkin, *Opt. Express* **2011**, *19*, 19942.
- [124] J. Chae, S. An, G. Ramer, V. Stavila, G. Holland, Y. Yoon, A. A. Talin, M. Allendorf, V. A. Aksyuk, A. Centrone, *Nano Lett.* **2017**, *17*, 5587.
- [125] A. M. Katzenmeyer, J. Canivet, G. Holland, D. Farrusseng, A. Centrone, *Angew. Chem., Int. Ed.* **2014**, *53*, 2852.
- [126] J. Chae, B. Lahiri, A. Centrone, *ACS Photonics* **2016**, *3*, 87.
- [127] A. B. Khanikaev, N. Arju, Z. Fan, D. Purtseladze, F. Lu, J. Lee, P. Sarriguren, M. Schnell, R. Hillenbrand, M. A. Belkin, G. Shvets, *Nat. Commun.* **2016**, *7*, 12045.
- [128] P. Li, M. Lewin, A. V. Kretinin, J. D. Caldwell, K. S. Novoselov, T. Taniguchi, K. Watanabe, F. Gaussmann, T. Taubner, *Nat. Commun.* **2015**, *6*, 7507.
- [129] Z. Fei, E. G. Iwinski, G. X. Ni, L. M. Zhang, W. Bao, A. S. Rodin, Y. Lee, M. Wagner, M. K. Liu, S. Dai, M. D. Goldflam, M. Thiemens, F. Keilmann, C. N. Lau, A. H. Castro-Neto, M. M. Fogler, D. N. Basov, *Nano Lett.* **2015**, *15*, 4973.
- [130] Z. Fei, A. S. Rodin, W. Gannett, S. Dai, W. Regan, M. Wagner, M. K. Liu, A. S. McLeod, G. Dominguez, M. Thiemens, H. C. NetoAntonio, F. Keilmann, A. Zettl, R. Hillenbrand, M. M. Fogler, D. N. Basov, *Nat. Nanotechnol.* **2013**, *8*, 821.
- [131] A. J. Giles, S. Dai, I. Vurgaftman, T. Hoffman, S. Liu, L. Lindsay, C. T. Ellis, N. Assefa, I. Chatzakis, T. L. Reinecke, J. G. Tischler, M. M. Fogler, J. H. Edgar, D. N. Basov, J. D. Caldwell, *Nat. Mater.* **2018**, *17*, 134.
- [132] B. Lahiri, G. Holland, V. Aksyuk, A. Centrone, *Nano Lett.* **2013**, *13*, 3218.
- [133] A. Ambrosio, L. A. Jauregui, S. Dai, K. Chaudhary, M. Tamagnone, M. M. Fogler, D. N. Basov, F. Capasso, P. Kim, W. L. Wilson, *ACS Nano* **2017**, *11*, 8741.
- [134] A. Centrone, *Annu. Rev. Anal. Chem.* **2015**, *8*, 101.
- [135] P. Pons-Valencia, F. J. Alfaro-Mozaz, M. M. Wiecha, V. Bielek, I. Dolado, S. Velez, P. Li, P. Alonso-Gonzalez, F. Casanova, L. E. Hueso, L. Martin-Moreno, R. Hillenbrand, A. Y. Nikitin, *Nat. Commun.* **2019**, *10*, 3242.
- [136] D. Nowak, W. Morrison, H. K. Wickramasinghe, J. Jahng, E. Potma, L. Wan, R. Ruiz, T. R. Albrecht, K. Schmidt, J. Frommer, D. P. Sanders, S. Park, *Sci. Adv.* **2016**, *2*, e1501571.
- [137] T. U. Tumkur, X. Yang, B. Cerjan, N. J. Halas, P. Nordlander, I. Thomann, *Nano Lett.* **2016**, *16*, 7942.
- [138] A. Ambrosio, R. C. Devlin, F. Capasso, W. L. Wilson, *ACS Photonics* **2017**, *4*, 846.
- [139] A. Politano, G. Chiarello, *Nanoscale* **2014**, *6*, 10927.
- [140] A. Losquin, T. T. A. Lummen, *Front. Phys.* **2017**, *12*, 127301.
- [141] A. Politano, G. Chiarello, *Prog. Surf. Sci.* **2015**, *90*, 144.
- [142] A. Politano, G. Chiarello, C. Spinella, *Mater. Sci. Semicond. Process.* **2017**, *65*, 88.

- [143] J. Lu, K. P. Loh, H. Huang, W. Chen, A. T. S. Wee, *Phys. Rev. B* **2009**, *80*, 113410.
- [144] A. Cupolillo, N. Ligato, L. S. Caputi, *Appl. Phys. Lett.* **2013**, *102*, 111609.
- [145] M. K. Kinyanjui, C. Kramberger, T. Pichler, J. C. Meyer, P. Wachsmuth, G. Benner, U. Kaiser, *EPL* **2012**, *97*, 57005.
- [146] V. B. Jovanović, I. Radović, D. Borka, Z. L. Mišković, *Phys. Rev. B* **2011**, *84*, 155416.
- [147] R. J. Wu, M. Topsakal, M. C. Robbins, N. Haratipour, J. S. Jeong, R. M. M. Wentzcovich, S. J. Koester, K. Andre Mkhoyan, *Microsc. Microanal.* **2015**, *21*, 109.
- [148] S. C. Liou, M. W. Chu, R. Sankar, F. T. Huang, G. J. Shu, F. C. Chou, C. H. Chen, *Phys. Rev. B* **2013**, *87*, 085126.
- [149] V. Mauchamp, M. Bugnet, E. P. Bellido, G. A. Botton, P. Moreau, D. Magne, M. Naguib, T. Cabioch, M. W. Barsoum, *Phys. Rev. B* **2014**, *89*, 235428.
- [150] A. Sumiyoshi, H. Hyodo, Y. Sato, M. Terauchi, K. Kimura, *Solid State Sci.* **2015**, *47*, 68.
- [151] K. L. Kostov, F. O. Schumann, S. Polzin, D. Sander, W. Widdra, *Phys. Rev. B* **2016**, *94*, 075438.
- [152] J. Tao, L. Wu, G. Zheng, *Carbon* **2018**, *133*, 249.
- [153] T. B. Tan, G. J. Ren, Y. Liu, Y. Q. Wang, J. Q. Yao, *Opt. Commun.* **2015**, *346*, 149.
- [154] S. Liu, C. Zhang, M. Hu, X. Chen, P. Zhang, S. Gong, T. Zhao, R. Zhong, *Appl. Phys. Lett.* **2014**, *104*, 201104.
- [155] S. Gong, T. Zhao, M. Sanderson, M. Hu, R. Zhong, X. Chen, P. Zhang, C. Zhang, S. Liu, *Appl. Phys. Lett.* **2015**, *106*, 223107.
- [156] T. Coenen, B. J. M. Brenny, E. J. Vesseur, A. Polman, *MRS Bull.* **2015**, *40*, 359.
- [157] M. Kuttge, E. J. R. Vesseur, A. F. Koenderink, H. J. Lezec, H. A. Atwater, F. J. García de Abajo, A. Polman, *Phys. Rev. B* **2009**, *79*, 113405.
- [158] J. Berson, M. Moosmann, S. Walheim, T. Schimmel, *Nano Lett.* **2019**, *19*, 816.
- [159] T. Coenen, E. J. R. Vesseur, A. Polman, *ACS Nano* **2012**, *6*, 1742.
- [160] T. Coenen, J. van de Groep, A. Polman, *ACS Nano* **2013**, *7*, 1689.
- [161] E. J. R. Vesseur, R. de Waele, M. Kuttge, A. Polman, *Nano Lett.* **2007**, *7*, 2843.
- [162] J. Y. Ou, J. K. So, G. Adamo, A. Sulaev, L. Wang, N. I. Zheludev, *Nat. Commun.* **2014**, *5*, 5139.
- [163] J. C. Long, H. W. Chan, A. B. Churnside, E. A. Gulbis, M. C. Varney, J. C. Price, *Nature* **2003**, *421*, 922.
- [164] R. C. Word, J. P. Fitzgerald, R. Konenkamp, *Opt. Express* **2013**, *21*, 30507.
- [165] L. Zhang, A. Kubo, L. Wang, H. Petek, T. Seideman, *Phys. Rev. B* **2011**, *84*, 245442.
- [166] L. Douillard, F. Charra, *J. Electron Spectrosc. Relat. Phenom.* **2013**, *189*, 24.
- [167] T. Leißner, K. Thilsing-Hansen, C. Lemke, S. Jauernik, J. Kjelstrup-Hansen, M. Bauer, H.-G. Rubahn, *Plasmonics* **2012**, *7*, 253.
- [168] P. Melchior, D. Bayer, C. Schneider, A. Fischer, M. Rohmer, W. Pfeiffer, M. Aeschlimann, *Phys. Rev. B* **2011**, *83*, 235407.
- [169] T. Lehnert, O. Lehtinen, G. Algara-Siller, U. Kaiser, *Appl. Phys. Lett.* **2017**, *110*, 033106.